JAMES | Journal of Advances in Modeling Earth Systems

RESEARCH ARTICLE
10.1029/2018MS001500

Special Section:
Community Earth System Model version 2 (CESM2) Special Collection

Implementing Plant Hydraulics in the Community Land Model, Version 5

Daniel Kennedy[1], Sean Swenson[2], Keith W. Oleson[2], David M. Lawrence[2], Rosie Fisher[2], Antonio Carlos Lola da Costa[3], and Pierre Gentine[1]

[1]Department of Earth and Environmental Engineering, Columbia University, New York, NY, USA, [2]National Center for Atmospheric Research, Boulder, CO, USA, [3]Centro de Geociências, Universidade Federal do Pará, Belém, Pará, Brazil

Abstract Version 5 of the Community Land Model (CLM5) introduces the plant hydraulic stress (PHS) configuration of vegetation water use, which is described and compared with the corresponding parameterization from CLM4.5. PHS updates vegetation water stress and root water uptake to better reflect plant hydraulic theory, advancing the physical basis of the model. The new configuration introduces prognostic vegetation water potential, modeled at the root, stem, and leaf levels. Leaf water potential replaces soil potential as the basis for stomatal conductance water stress, and root water potential is used to implement hydraulic root water uptake, replacing a transpiration partitioning function. Point simulations of a tropical forest site (Caxiuanã, Brazil) under ambient conditions and partial precipitation exclusion highlight the differences between PHS and the previous CLM implementation. Model description and simulation results are contextualized with a list of benefits and limitations of the new model formulation, including hypotheses that were not testable in previous versions of the model. Key results include reductions in transpiration and soil moisture biases relative to a control model under both ambient and exclusion conditions, correcting excessive dry season soil moisture stress in the control model. PHS implements hydraulic gradient root water uptake, which allows hydraulic redistribution and compensatory root water uptake and results in PHS utilizing a larger portion of the soil column to buffer shortfalls in precipitation. The new model structure, which bases water stress on leaf water potential, could have significant implications for vegetation-climate feedbacks, including increased sensitivity of photosynthesis to atmospheric vapor pressure deficit.

Key Points:
- An updated soil-plant-atmosphere continuum model based on hydraulic theory is implemented in the Community Land Model (version 5)
- Prognostic leaf water potential replaces soil matric potential as the basis for stomatal conductance water stress
- Prognostic root water potential is used to implement hydraulic root water uptake, replacing a "soil wilting point" approach

Supporting Information:
- Supporting Information S1

Correspondence to:
D. Kennedy,
djk2120@columbia.edu

Citation:
Kennedy, D., Swenson, S., Oleson, K. W., Lawrence, D. M., Fisher, R., Lola da Costa, A. C., & Gentine, P. (2019). Implementing plant hydraulics in the Community Land Model, version 5. *Journal of Advances in Modeling Earth Systems*, *11*, 485–513. https://doi.org/10.1029/2018MS001500

Received 14 SEP 2018
Accepted 26 JAN 2019
Accepted article online 31 JAN 2019
Published online 15 FEB 2019

1. Introduction

Trees face emerging risk from climate change globally, which may lead to increases in mortality and decreases in the terrestrial carbon sink (Allen et al., 2010; Anderegg et al., 2013; McDowell et al., 2016). In addition to stress from soil moisture drought, vegetation is susceptible to increasing atmospheric demand for evapotranspiration (Lemordant et al., 2018; Novick et al., 2016; Restaino et al., 2016). Increases in vapor pressure deficit (VPD) are occurring with global warming (Ficklin & Novick, 2017; Seager et al., 2015) and are associated with impacts on vegetation, such as large-scale die-off (McDowell & Allen, 2015; A. P. Williams et al., 2013). Understanding vegetation response to environmental drivers is important both for discerning future climate impacts on forests and for modeling feedbacks to the carbon and hydrological cycles (Lemordant et al., 2018). Significant uncertainty remains in Earth System Model (ESM) predictions of the carbon cycle, partly attributed to the response of vegetation to changes in hydroclimate (De Kauwe et al., 2017; Friedlingstein et al., 2014; Trugman et al., 2018).

Soil moisture stress (SMS) parameterizations are used by ESMs to determine the regulation of surface fluxes (photosynthesis and transpiration) by vegetation in response to water fluctuations (Egea et al., 2011; Verhoef & Egea, 2014). Such parameterizations relate a metric of soil moisture status to leaf gas exchange, defining the response of stomatal conductance to declining soil water, serving to attenuate transpiration, photosynthesis, and root water uptake (RWU) with drying. Water stress dynamics have broad effects on critical land surface processes within models (Joetzjer et al., 2014), such as evapotranspiration. Likewise, because vegetation water use strategies modulate carbon uptake, creating a close coupling between the Earth system's carbon and hydrological cycles (Green et al., 2017), vegetation water stress regulates the global carbon cycle. This occurs on seasonal and interannual timescales, with stress attenuating transpiration (De Kauwe et al., 2015) and photosynthesis (Stocker et al., 2018). Furthermore, water stress parameterizations influence

the diurnal cycle, through the partitioning of latent versus sensible heat, modifying the Bowen ratio (Gentine et al., 2007, 2011). This in turn feeds back onto surface and air temperature, through land-atmosphere feedbacks (Bonan, 2008; Seneviratne et al., 2006). Recent studies have shown that SMS functions are a major driver of uncertainty in leaf gas exchange in ESMs (Trugman et al., 2018) and can systematically overestimate the effect of soil moisture drought on evaporative fluxes (Bonan et al., 2014; Ukkola et al., 2016). In Amazonia, which is the focus area of our model test runs, studies suggest that the CLM (version 3.5) simultaneously underestimates the effect of experimental drought treatment (Powell et al., 2013) and overestimates dry season reductions in gross primary productivity (GPP; Restrepo-Coupe et al., 2017).

More mechanistic representations of stress and vegetation water use dynamics have been achieved by incorporating plant hydraulic theory into land surface models, modeling water flow throughout the soil-plant-atmosphere continuum (SPAC; Christoffersen et al., 2016; Sperry et al., 2017; Xu et al., 2016). Explicit modeling of water flow through the vegetation substrate increases model complexity but is consistent with evidence of dynamic regulation of vegetation water use in response to both soil and atmospheric drying (Sperry et al., 1998; Sperry & Love, 2015; Tardieu & Simonneau, 1998). Furthermore, because they are based on Darcy's law, plant hydraulic models have a robust physical basis compared to models that utilize empirical water stress formulations. Plant hydraulic models involve new parameters, which may prove challenging to constrain (Drake et al., 2017), but plant hydraulic trait data are available (Anderegg, 2015; Kattge et al., 2011), providing constraints on parameter estimation. Such trait data have been shown to improve predictions of species vulnerability to drought (Anderegg, Konings, et al., 2018; Choat et al., 2012; Giardina et al., 2018; Mackay et al., 2015; Powell et al., 2018). Likewise, vegetation water status observations are now available from remote sensing platforms, at a scale that is directly comparable to model development (Grant et al., 2016; Konings et al., 2016) and therefore can be used to validate model results (Konings et al., 2017; Momen et al., 2017).

In this study, we develop a new plant water stress parameterization based on hydraulic theory within the recently released Community Land Model, version 5 (CLM5, the land component of the Community Earth System Model, version 2). We refer to this hydraulics-based implementation as the “plant hydraulic stress” (PHS) configuration. Previous versions of the CLM employed an empirical SMS function, as described above.

PHS, by explicitly representing plant hydraulics, introduces modeled vegetation water potential (discretized into leaf, stem, and root elements) into the CLM, as well as a physical model of water supply, from the soil through the vegetation substrate. Transpiration is attenuated in the model based on leaf water potential, capturing dynamic vegetation water use regulation in response to both soil moisture and atmospheric evaporative demand. These changes in the parameterization framework have numerous implications, including the following:

1. Leaf water potential serves as a metric for plant water status instead of soil water or soil matric potential. As such, it reflects vegetation sensitivity to both soil and atmospheric drying, while serving as a diagnostic for excessive xylem tension and cavitation risk.
2. Using a Darcy's law approximation to model plant hydrodynamics allows representation of hydraulic redistribution (HR; Lee et al., 2005), as water fluxes are always directed down gradients of water potentials.
3. Root water potential can be used to predict gradient-based RWU approximated by Darcy's law, replacing the previous empirical transpiration partitioning heuristic. This provides the means to vary, for example, the mean depth of extraction with changing soil water conditions.
4. Representation of a range of water use strategies (e.g., isohydricity and anisohydricity), improving the connection between leaf gas exchange and water availability.
5. Modeling vegetation water potential allows improved connection to remote sensing observations of vegetation water status (vegetation optical depth; Konings et al., 2016).

To assess the new model formulation, we carried out site-level simulations at Caxiuanã National Forest in Brazil, a terra-firme moist tropical evergreen forest (Fisher et al., 2006). Starting in 2001, a plot at this site was subjected to an approximately 50% precipitation throughfall exclusion. Due to the large drop in soil moisture at the precipitation exclusion site, significant vegetation water stress regulation of transpiration and photosynthesis was observed (da Costa et al., 2010, 2014), providing a drought signal to demonstrate model dynamics (Fisher et al., 2007).

In this paper we therefore introduce the PHS theory and implementation in the CLM (section 2); describe the details of the experiment setup (section 3); analyze the dynamics of modeled water stress, RWU, transpiration, and soil moisture profiles (section 4); discuss differences between PHS and the previous CLM water stress configuration (section 5); and outline the benefits and limitations of the new model (section 5.5).

2. Model Description

This study develops a new parameterization of water stress (sections 2.4.1 and 2.5.1) and RWU (sections 2.4.2 and 2.5.2) within the CLM. We use two configurations of CLM5 to compare the new parameterization with the corresponding parameterization from CLM4.5. The new parameterization is called PHS; PHS is the default configuration of CLM5. The alternative configuration, which we refer to as SMS, deploys the CLM4.5 default RWU and water stress implementations within CLM5. In sections 2.1–2.3, we describe the components that the two configurations share in common. In sections 2.4 and 2.5, we describe their differences.

2.1. Stomatal Conductance

CLM5 implements the Medlyn stomatal conductance model (Franks et al., 2018; Medlyn et al., 2011), which reconciles the empirical approach to modeling stomatal conductance with a carbon-water optimization framework (Cowan & Farquhar, 1977). The Cowan and Farquhar (1977) optimization requires plants to maximize photosynthesis relative to transpiration costs, which the Medlyn model captures in an empirically tractable form (equation (1)). Stomatal conductance of water (g_s) is directly related to net photosynthesis (A_n) and inversely related to the square root of the VPD near the leaf surface ($\sqrt{D}$) and the concentration of CO_2 at the leaf surface (C_a).

$$g_s = g_0 + 1.6\left(1 + \frac{g_1}{\sqrt{D}}\right)\frac{A_n}{C_a}. \tag{1}$$

The model features two parameters: g_0 (μmol/m^2/s) and g_1 (kPa$^{0.5}$). The g_0 parameter is the minimum stomatal conductance, representing cuticular and epidermal losses (small). The g_1 parameter relates to the marginal water cost guiding the optimization of carbon assimilation. These parameters are plant functional type dependent.

While maximizing assimilation relative to water transpiration costs, the Medlyn model does not resolve concurrent limitations to stomatal conductance associated with declining soil water (such as in Manzoni et al., 2013) or excessive xylem tension. To represent such water stress, and its impact on leaf gas exchange, land surface models typically include a "water stress factor." The PHS implementation follows this approach, using the Medlyn model to calculate stomatal conductance absent water stress, which is attenuated as leaf water potential declines (see section 2.3). More recent stomatal conductance models eschew the Cowan and Farquhar (1977) optimization in favor of a framework to maximize carbon assimilation relative to hydraulic costs (Anderegg, Wolf, et al., 2018; Sperry et al., 2017; Wolf et al., 2016), which directly incorporate leaf water potential and hydraulic safety margin (HSM) into the stomatal conductance formulation. Such models do not require a water stress factor and should be tested for future versions of PHS.

2.2. Photosynthesis

The CLM5 photosynthesis model is described in detail in Bonan et al. (2011), Thornton and Zimmermann (2007), and Oleson et al. (2013). Photosynthesis is limited by three factors: carboxylation-limitations, light-limitations, and export-limitations following Farquhar et al. (1980) and Harley et al. (1992). Water stress (as discussed in the next section) is applied within the carboxylation-limited regime, by attenuating the maximum rate of carboxylation (V_{cmax}). The implementation extends (Sellers, Randall, et al., 1996; Sellers, Tucker, et al., 1996) with colimitation following Collatz et al. (1991).

The CLM5 photosynthesis module, in its default configuration, is a two-big-leaf model, with a sunlit and shaded leaf for each plant functional type (Dai et al., 2004; Oleson et al., 2013; Thornton & Zimmermann, 2007). The canopy fluxes module iterates the solution for leaf temperatures to satisfy the leaf surface energy balances on both sunlit and shaded leaves, in response to forcing conditions. Within this, the photosynthesis module further iterates to solve for stomatal conductance and intercellular CO_2 concentration, balancing stomatal flux of CO_2 with photosynthetic assimilation flux of CO_2 (see Figure A1 for a flow chart of these iterations).

2.3. Water Stress Factor

Uncertainty remains within the literature as to how and where to apply water stress factors to photosynthesis and/or stomatal conductance (Novick et al., 2016; Sperry & Love, 2015; Zhou et al., 2013). In the CLM, the water stress factor (f_w) multiplies the "well-watered rate" of maximum carboxylation ($V_{\mathrm{cmax,ww}}$) to effect water stress (as described in Oleson et al., 2013).

$$V_{\mathrm{cmax}} = f_w V_{\mathrm{cmax,ww}}. \tag{2}$$

Attenuating V_{cmax} is not the only method for incorporating a response to declining water availability. Other models opt to apply water stress directly to stomatal conductance, linking the stomatal conductance model slope parameter to soil moisture (e.g., De Kauwe et al., 2015). However, Lin et al. (2018) found that only the intercept parameter and photosynthesis (through changes in light-use efficiency) were sensitive to soil moisture based on eddy covariance observations and not the slope parameter. Furthermore, Zhou et al. (2013) suggest that changes in assimilation tend to exceed those predicted by modulating g_1 with soil moisture, but could be captured by changing V_{cmax}. These results would thus suggest that it is appropriate to modulate V_{cmax}. Other field studies, however, suggest that measured V_{cmax} at the leaf level does not change with drought (Flexas et al., 2004). On the other hand, the modeled V_{cmax} is a bulk measure of V_{cmax} and may implicitly account for mesophyll conductance changes (Rogers et al., 2017), which has been shown to be water stress dependent (Flexas et al., 2012).

For now, applying water stress through V_{cmax} seems well supported, but future refinements may be appropriate. In this study, we preserve the method of applying water stress used in CLM4.5, while instead experimenting with how f_w responds to environmental conditions.

2.4. SMS (CLM4.5 Default)

2.4.1. SMS Water Stress Factor

In SMS, f_w is calculated as the summation of a soil layer wilting factor (w_i) across the n soil layers, weighted by root fraction (r_i) (Oleson et al., 2013). The soil wilting factor is a bounded linear function of soil matric potential ($\psi_{\mathrm{soil},i}$). The function is defined by two parameters, the soil potential at (and above), which stomates are fully open (ψ_o), and the value at which stomates are fully closed (ψ_c).

$$f_{w,\mathrm{SMS}} = \sum_{i=1}^{n} r_i w_i \tag{3}$$

$$w_i = 0 \leq \frac{\psi_{\mathrm{soil},i} - \psi_c}{\psi_o - \psi_c} \leq 1 \tag{4}$$

2.4.2. SMS RWU

The CLM features a vertically discretized soil column with variable soil layer thicknesses. The number of soil layers (n) can vary, depending on the depth to bedrock. Soil water movement in each soil layer is governed by Richards' equation, with RWU (q_i) incorporated as a sink term. Summed over the soil column, RWU is required to equal transpiration (T).

$$T = \sum_{i}^{n} q_i \tag{5}$$

In the SMS configuration, a heuristic function (based on $f_{w,\mathrm{SMS}}$) is used to determine q_i. Transpiration is partitioned among the soil layers based on the product of the root fraction and the wilting factor, which is then normalized by $f_{w,\mathrm{SMS}}$ to satisfy equation (5). Because the relative root fractions are used to partition transpiration, RWU is not connected to absolute root biomass. For example, if root biomass doubles in every soil layer, the relative root fractions do not change, with no impact on modeled soil water availability.

$$q_i = \frac{r_i w_i}{f_{w,\mathrm{SMS}}} T. \tag{6}$$

Substituting for w_i yields the SMS RWU equation as a function of the layer-i soil potential ($\psi_{\mathrm{soil},i}$).

$$q_i = \begin{cases} 0 & \text{if } \psi_{\text{soil},i} < \psi_c \\ \frac{T}{f_{w,\text{SMS}}} \frac{r_i}{\psi_o - \psi_c} \left(\psi_{\text{soil},i} - \psi_c\right) & \text{if } \psi_c \le \psi_{\text{soil},i} \le \psi_o \\ \frac{T}{f_{w,\text{SMS}}} r_i & \text{if } \psi_{\text{soil},i} > \psi_o \end{cases} . \tag{7}$$

In the Darcy framework, water fluxes are the product of hydraulic conductance (k_i) and hydraulic gradient ($\Delta\psi$). Although SMS does not explicitly calculate hydraulic conductance, equation (7) can be used to define hydraulic analogs resulting from the transpiration partitioning heuristic function, allowing easier comparison to the PHS RWU implementation.

$$\begin{aligned} q_i &= -k_i \Delta\psi \\ \Delta\psi &= \psi_c - \psi_{\text{soil},i} \\ k_i &= \frac{T}{f_{w,\text{SMS}}} \frac{r_i}{\psi_o - \psi_c} \\ \text{constrained by} \quad \Delta\psi &= \begin{cases} 0 & \text{if } \psi_{\text{soil},i} < \psi_c \\ \psi_c - \psi_o & \text{if } \psi_{\text{soil},i} > \psi_o \end{cases} \end{aligned} \tag{8}$$

2.5. PHS (CLM5 Default)

2.5.1. PHS Water Stress Factor

HS introduces a new formulation for f_w, which is based on leaf water potential (ψ_{leaf}) instead of soil potential (described further in section 2.5.5). The relationship is modeled with a sigmoidal function, subject to two parameters: the water potential at 50% loss of stomatal conductance (p_{50}) and a shape-fitting parameter (c_k).

$$f_{w,\text{PHS}} = 2^{-\left(\frac{\psi_{\text{leaf}}}{p_{50}}\right)^{c_k}} \tag{9}$$

$$\psi_{\text{leaf}} = \psi_{\text{soil}} + \Delta\psi \tag{10}$$

Utilizing leaf water potential has been shown to improve stomatal models (Anderegg et al., 2017) and reflects hydraulic limits on plant transpiration (Manzoni et al., 2013; Sperry et al., 1998). Leaf water potential is modulated by supply of sap to the leaves and by evaporative demand, as regulated by stomatal dynamics (Sperry & Love, 2015). As a result, low soil water induces stress due to limited water supply, but in addition, high atmospheric VPD can induce stress with the associated increases in the gradient in water potential across the plant xylem. This latter mechanism was absent from the previous water stress function (dependent on soil water potential only), by construction. Given the observed increase in VPD with global warming, it appears critical to include such mechanistic dependence of water stress (Novick et al., 2016). While the Medlyn stomatal conductance model does depend on VPD, the model does not (given constant g_1) reflect the risk of hydraulic failure (Zhou et al., 2013). The new stress factor formulation reflects the dual risks of soil moisture deficit and atmospheric demand on hydraulic safety (A. P. Williams et al., 2013), requiring vegetation to avoid excessive xylem tension associated with risk of cavitation.

2.5.2. PHS RWU

PHS implements an alternative to the SMS heuristic approach for RWU, using a mechanistic representation utilizing Darcy's law for flow through porous media to approximate the vegetation water fluxes. Instead of a constant parameter (ψ_c) defining the gradient in water potential within the SMS hydraulic analogy (equation (8)), PHS implements a physical model of vegetation water potential (details in section 2.5.3). The water flux from a given soil layer is driven by the gradient between soil potential ($\psi_{\text{soil},i}$) and the water potential in the root collar (ψ_{root}), after accounting for the effects of gravity ($\rho g z_i$, where z_i is the soil layer depth). Hydraulic conductance across the soil and roots (k_{sr}) is modeled based on soil hydraulic properties and xylem vulnerability, accounting for both the path across the soil matrix and through the xylem conduits. Furthermore, in lieu of using relative root fraction (as in SMS), k_{sr} depends on the root area index (RAI), an absolute measure of root abundance (details in Appendix A).

$$q_i = -k_{\text{sr},i} \left(\psi_{\text{root}} - \psi_{\text{soil},i} + \rho g z_i\right) \tag{11}$$

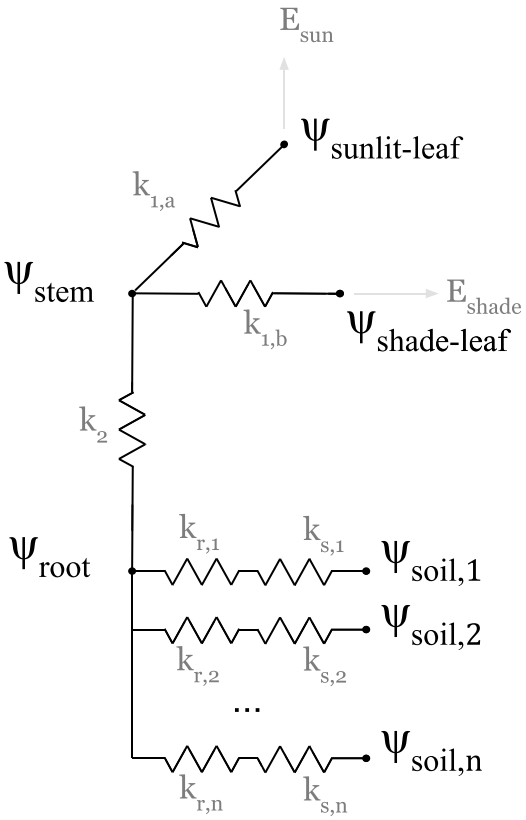

Figure 1. Plant hydraulic circuit analog schematic.

2.5.3. Modeling Vegetation Water Potential

The PHS model within CLM5 uses Darcy's law to approximate the flow of water through the SPAC, which can be represented with an electrical circuit analogy (Figure 1). PHS solves for vegetation water potential along the path from soil-to-atmosphere. Vegetation water supply and demand are both coupled to vegetation water potential, as described in the previous two sections. The solution for vegetation water potential is the set of values that matches supply with demand, maintaining water balance across each of the vegetation water potential nodes.

PHS solves for vegetation water potential at four locations: ψ_{root}, ψ_{stem}, $\psi_{\text{shade-leaf}}$, and $\psi_{\text{sun-leaf}}$. The number of nodes is chosen as the strict minimum to allow for differences in segment parameterizations (Simonin et al., 2015; Sperry & Love, 2015) while also conforming to existing CLM model structure (vertically discretized soil layers, two-big-leaf). At each node in the circuit diagram (Figure 1), we model water potential, and, between nodes, we resolve the flux of water based on Darcy's law. Water uptake from the different soil layers is assumed to operate in parallel: a typical assumption justified by higher resistance in lateral versus central roots (e.g., M. Williams et al., 2001). Two resistors operate in series between each ψ_{soil} and ψ_{root}, to represent the path across the soil matrix and then through the root tissue (M. Williams et al., 1996). Specifics on the parameterization of hydraulic conductance for each segment are provided in Appendix A1. Solving for vegetation water potential requires matching vegetation water supply (RWU, sap flux through the stem) with vegetation water demand (sunlit and shaded leaf transpiration).

2.5.4. Water Supply

Water supply is modeled via Darcy's law, where the flux of water (q) is the product of the path hydraulic conductance (k) and the gradient in water potential ($\psi_2 - \psi_1$) after accounting for gravitational potential ($\rho g \Delta z$). Equation (12) represents the flow from a generic node 1 to node 2.

$$q = -k\left(\psi_2 - \psi_1 + \rho g \Delta z\right). \tag{12}$$

For simplicity, PHS does not represent plant tissue water storage (or capacitance, using the electrical circuit analogy), which is in line with recent supply-loss theory (Sperry & Love, 2015). Capacitance significantly

complicates the water potential solution (Celia et al., 1990) and is challenging to parameterize (Bartlett et al., 2016). However, buffering of water stress provided by tissue water storage could potentially be important especially on subdaily timescales (Epila et al., 2017; Meinzer et al., 2009), whereby its inclusion may be warranted in future model versions.

Hydraulic conductance through vegetation segments is modeled following empirical xylem vulnerability curves (Tyree & Sperry, 1989), where segments lose conductance with increasing xylem tension related to cavitation and embolism (Holbrook et al., 2001). The vulnerability curves model loss of conductance relative to maximum conductance ($k_{\max}$) using two parameters: c_k, a sigmoidal shape-fitting parameter, and p_{50}, the water potential at 50% loss of segment conductance (following Gentine et al., 2016).

$$k = k_{\max} 2^{-\left(\frac{\psi_1}{p_{50}}\right)^{c_k}}. \tag{13}$$

Both c_k and p_{50} can be estimated from field experiments (Sack et al., 2002), and p_{50} is available in the TRY trait database (Kattge et al., 2011). Parameterization based on p_{50} aligns with the call for a transition to models that use a wider range of plant functional trait data in their parameterization (Anderegg, 2015). The loss of xylem conductivity is based on lower terminal water potential (ψ_1) as is typical in other simplified models (Xu et al., 2016) but may underestimate the integrated loss of conductivity (Sperry & Love, 2015). This bias could underestimate hydraulic limits on gas exchange and/or affect parameter estimation (e.g., requiring lower $k_{\max}$). Likewise, xylem are assumed to symmetrically regain conductance, which may lead to underestimating persistent drought legacies (Anderegg et al., 2015). PHS was explicitly designed as a simplified model that can be refined in future versions.

PHS models root, stem, and leaf tissue conductances according to equation (13). The parameterization of $k_{\max}$ varies by hydraulic segment (see details in Appendix A1). The conductances across the soil matrix ($k_{s,1}, \ldots, k_{s,n}$) to the root surface follows M. Williams et al. (2001) and Bonan et al. (2014), which scales soil conductivity (Brooks & Corey, 1964; Clapp & Hornberger, 1978) by an appropriate conducting distance based on the root distribution. Details are provided in Appendix A1.

2.5.5. Water Demand

Water demand is calculated using the Medlyn stomatal conductance model (see section 2.1) modulated by the CLM water stress factor. As discussed earlier f_w is based on leaf water potential in PHS, where stress increases as leaf water potential becomes more negative (Klein & Niu, 2014). Emerging from this new stress formulation is a connection between drought stress and HSM, which measures the difference between the minimum leaf water experienced by vegetation and the water potential at a given percent loss of conductivity (e.g., $HSM = p_{50} - \psi_{\text{leaf,min}}$). Variations in HSM have been shown to explain a significant portion of the variance in ecosystem drought sensitivity (Anderegg, Konings, et al., 2018).

$$\begin{aligned} f_{w,\text{sun}} &= 2^{-\left(\frac{\psi_{\text{sun-leaf}}}{p_{50}}\right)^{c_k}} \\ f_{w,\text{shade}} &= 2^{-\left(\frac{\psi_{\text{shade-leaf}}}{p_{50}}\right)^{c_k}} \end{aligned} \tag{14}$$

Because leaf water potential is modeled separately for sunlit and shaded leaves, f_w takes on distinct sunlit and shaded values. Shaded and sunlit leaf transpiration ($E_{\text{sun}}, E_{\text{shade}}$) are calculated by attenuating maximal transpiration ($E_{\text{sun,max}}, E_{\text{shade,max}}$) according to f_w. $E_{\text{sun,max}}$ and $E_{\text{shade,max}}$ are calculated at the beginning of each time step by running the stomatal conductance model with $f_w = 1$. Equations (14) and (15) reflect a simplification used within iterations of the PHS module, neglecting nonlinear components of the relationship between stress and transpiration (which is resolved through iteration, as described in Appendix section A1).

$$\begin{aligned} E_{\text{sun}} &= f_w E_{\text{sun,max}} \\ E_{\text{shade}} &= f_w E_{\text{shade,max}} \end{aligned} \tag{15}$$

2.5.6. PHS Solution

PHS solves for the set of vegetation water potential values (ψ) that matches water supply (RWU) to water demand (transpiration), while satisfying continuity across the four water flow segments (soil-to-root, root-to-stem, stem-to-leaf, and leaves-to-transpiration). Beginning from an initial condition of ψ (from the

previous time step), PHS computes the flux divergence f (representing the mismatch of flow in and out of each segment) and iteratively updates ψ until it reaches convergence; that is, $f \to 0$.

$$\psi = \begin{bmatrix} \psi_{\text{sun}} \\ \psi_{\text{shade}} \\ \psi_{\text{stem}} \\ \psi_{\text{root}} \end{bmatrix} \tag{16}$$

$$f(\psi) = \begin{bmatrix} E_{\text{sun}} - q_{\text{sun}} \\ E_{\text{shade}} - q_{\text{shade}} \\ q_{\text{sun}} + q_{\text{shade}} - q_{\text{stem}} \\ q_{\text{stem}} - \sum_{j=1}^{n} q_{\text{root},j} \end{bmatrix} \tag{17}$$

$$A = \frac{\mathrm{d}f}{\mathrm{d}\psi} \tag{18}$$

While $|f| > 0$

$$\begin{aligned} \Delta\psi &= A^{-1} f\left(\psi_i\right) \\ \psi_{i+1} &= \psi_i + \Delta\psi \end{aligned} \tag{19}$$

The numerics are tractable because f has continuous, analytical derivatives and A (a 4×4 matrix with six null entries) is easy to invert when well conditioned. Supply and demand converge, because transpiration demand decreases with more negative leaf water potentials and supply increases with more negative leaf water potentials. The PHS loop is nested within iterations for intercellular CO_2 concentration and leaf temperature. Details on the numerical implementation are provided in Appendix section A1.

3. Experiment Description

We use a set of four simulations to demonstrate the impact of the plant hydrodynamics model (PHS versus SMS) on a tropical rainforest site, under ambient conditions and partial precipitation throughfall exclusion. This site is located in Eastern Amazonia (Caxiuanã, Brazil) and part of the Large-Scale Biosphere-Atmosphere Experiment in the Amazon (Avissar et al., 2002).

1. SMS, with ambient precipitation throughfall (AMB)
2. SMS, with 60% of precipitation throughfall excluded (TFE)
3. PHS, AMB
4. PHS, TFE

All four simulations use the same version of CLM5 (development version r270, www.github.com/ESCOMP/ctsm/releases/tag/clm4_ 5_ 18_ r270), which features a switch that can toggle between SMS and PHS configurations. Simulations are run off-line (uncoupled from an active atmospheric model), spanning from 2001 through 2003, utilizing the satellite phenology mode of CLM5 in which vegetation state (leaf area index [LAI] and canopy height) is prescribed and biogeochemistry is inactive. Six-year spin-up simulations (one each for SMS and PHS) are used to create initial conditions, repeating the ambient simulation twice. This satisfied steady state soil conditions, with soil matric potential changing by less than 0.2% between the two loops. Descriptions of site characteristics, forcing data, and observational sap flux and soil moisture can be found in Fisher et al. (2007, 2008).

3.1. Parameter Values and Throughfall Exclusion

Parameter values concerning vegetation hydrodynamics are presented in Table 1. All other parameters use the default values associated with the r270 version of CLM5. Informed by parameter values reported in Fisher et al. (2008), we tuned soil hydraulic parameters and the throughfall exclusion rate, to improve simulated soil moisture relative to observations (Figure S9 in the supporting information). An ensemble of simulations was used to tune the parameters for the PHS configuration to reasonably reflect sap flux observations (see Appendix A4).

Table 1
Select Parameter Values

CLM name	Full name	Symbol	Value
kmax(1)	Maximum Sun branch conductance	$k_{\text{sun,max}}$	4E−8 s^{-1}
kmax(2)	Maximum shade branch conductance	$k_{\text{shade,max}}$	4E−8 s^{-1}
kmax(3)	Maximum stem conductivity	$k_{\text{stem,max}}$	4E−8 m/s
krmax	Maximum root conductivity	$k_{r,\text{max}}$	6E−9 m/s
psi50	Water potential at 50% loss of conductivity	p_{50}	−1.75 MPa
ck	Vulnerability shape parameter	c_k	2.95
smpso	Soil potential with stomata fully open	ψ_o	−0.65 MPa
smpsc	Soil potential with stomata fully closed	ψ_c	−2.5 MPa
medlyn_intercept	Medlyn intercept	g_0	100 μmol/m^2/s
medlyn_slope	Medlyn slope	g_1	6 $kPa^{0.5}$
n	Soil porosity to 4.64 m	n	0.42
n	Soil porosity beyond 4.64 m	n	0.28
hksat	Saturated soil hydraulic conductivity	$k_{\text{s,max}}$	3E−5 m/s
sucsat	Saturated soil matric potential	ψ_{sat}	461 Pa
bsw	Brooks-Corey parameter	b	6

4. Results

4.1. Comparison With Observations

We tested two configurations of CLM5 (PHS and SMS) with simulations of the Caxiuanã throughfall exclusion experiment over 2001–2003. We compared modeled transpiration with observations derived from sap flux velocity and modeled soil moisture with observations using time domain reflectometry sensors (see above for experiment and observation details).

4.1.1. Transpiration, Ambient Conditions

Under ambient conditions, PHS reduces error and improves correlation between modeled and observed transpiration (compared to SMS, Figures 2a and 2c). While the two models make a similar number of small errors, SMS commits more errors exceeding 1 mm/day. The absolute value of SMS-OBS transpiration (Figure S3g) exceeds 1 mm/day in 67 of 414 days with available observations, as compared to just 23 with PHS. And while PHS error is limited to a maximum of 1.6 mm/dy, SMS error exceeds 2 mm/day 12 times. These 12 SMS errors all result from underestimating transpiration relative to observations, coinciding with dry soils, which is discussed further in section 5.4.

While PHS offers improvements modeling transpiration as measured by root-mean-square error (RMSE) and correlation, the ambient simulation seems to underestimate transpiration variability, with a standard deviation of daily transpiration of 0.61 mm/day compared to 0.87 mm/day in the observations (with SMS, the standard deviation is 0.97 mm/day). As such, PHS features a low bias for high transpiration values and a high bias for low transpiration values (Figure 2c). The difference in modeled transpiration between PHS and SMS derives from divergent water stress dynamics, which are discussed in section 5.2.

4.1.2. Transpiration, TFE

PHS performs better than SMS at reproducing transpiration observations under TFE (Figures 2b and 2d), featuring a higher R^2 (0.45 vs. 0.3) and lower RMSE (0.74 vs. 1.03 mm/day). However, both implementations show degraded results under TFE as compared to ambient rainfall conditions. Simulating the wet season under TFE (February-March-April) is prone to high transpiration biases in both models, where, in the observations, transpiration is reduced 32% by TFE, as compared to modeled reductions of only 1.6 and 4% for PHS and SMS, respectively. This may indicate that the models' sensitivity to soil potential declines are underestimated, or that water drains from the root zone more quickly after precipitation events than we represent with the soil hydraulic parameters (Figures 3b and 3d). Difficulty reproducing the effect of TFE (and the influence of soil moisture on leaf gas exchange) at Caxiuanã has precedent in the literature (Powell et al., 2013; Restrepo-Coupe et al., 2017).

4.1.3. Soil Moisture

The second source of observations for model evaluation is volumetric soil moisture. These data are used to evaluate the parameterization of RWU. Modeled soil moisture values (at a depth of 50 cm) are comparable

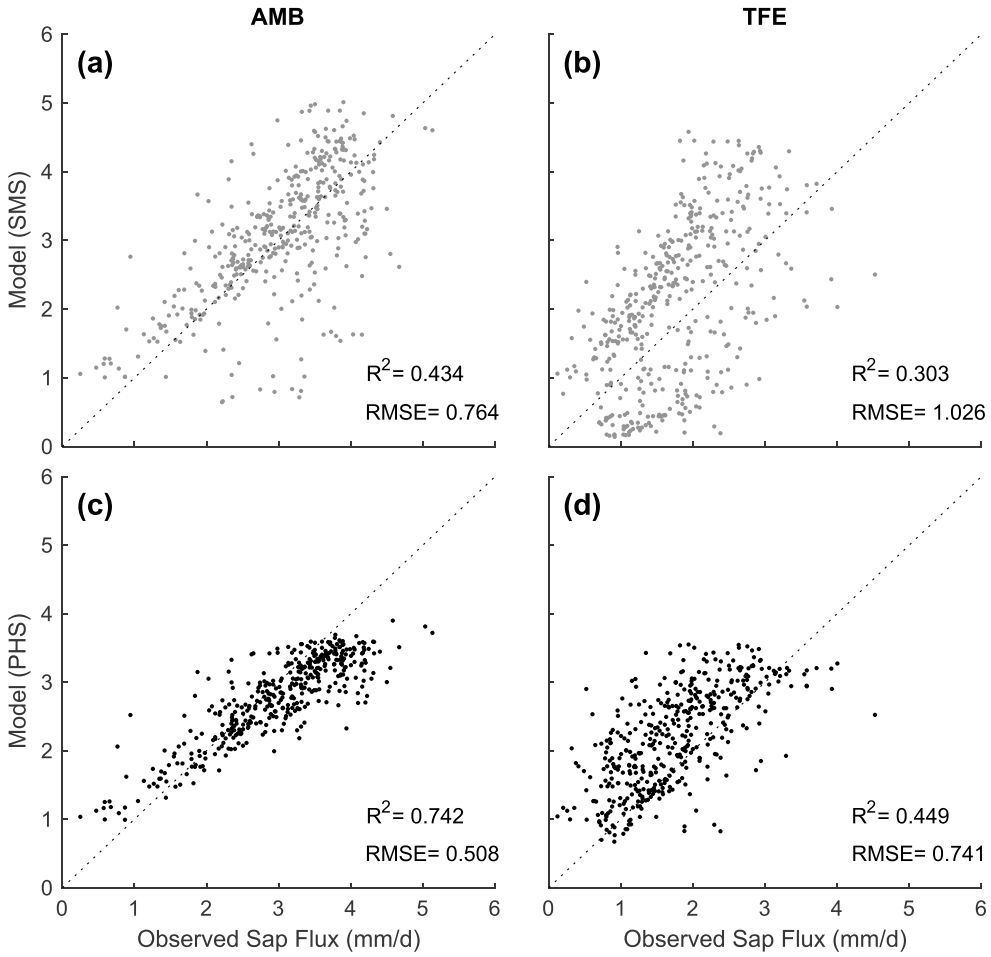

Figure 2. Modeled versus observed daily total transpiration. Observations are derived from field observations of sap flux velocity (see section 3). (a, b) SMS configuation, under ambient conditions and 60% TFE. (c,d) PHS configuation, under ambient conditions and 60% TFE. RMSE = root-mean-square error; SMS = soil moisture stress; PHS = plant hydraulic stress; TFE = throughfall excluded; AMB = ambient precipitation throughfall.

between model configurations during the wet season (February-March-April) under ambient conditions, both yielding averages of 28% (Figures 3a and 3c). With excess rainfall, soil moisture is largely determined by the soil field capacity and saturated conductivity, which are the same in both model configurations. With water shortfalls, the RWU parameterizations drive the soil moisture dynamics, and the models diverge, as SMS consistently generates lower soil moisture values (than PHS) within the first meter of the soil column (Figures 3 and S11). Soil moisture averages to 10% during the dry season (September-October-November, ambient case, depth = 50 cm) with SMS, as compared to 16% with PHS. PHS better comports with observations, reducing RMSE by 57% relative to SMS (Figures 3a and 3c).

We highlight the soil moisture at 50-cm depth, but similar patterns are observed throughout the first meter of the soil column (Figure S11). The 50-cm depth emphasizes the effect of modeled RWU, because it features higher root fraction than the deeper soil layers (Figure S1), but avoids the high-frequency dynamics of the top soil layer from soil evaporation and precipitation events that do not relate to differences between PHS and SMS. Under TFE, SMS minimum soil moisture is again 10% but holds there for a longer duration (Figure 3). Contrastingly, PHS achieves lower dry season soil moisture values under TFE as compared to ambient conditions. PHS better comports with observations, reducing RMSE by 42% relative to SMS (Figures 3a and 3c); however, both models seem to feature a high bias in soil moisture in the root zone (under TFE) during the wet season (Figures 3 and S11).

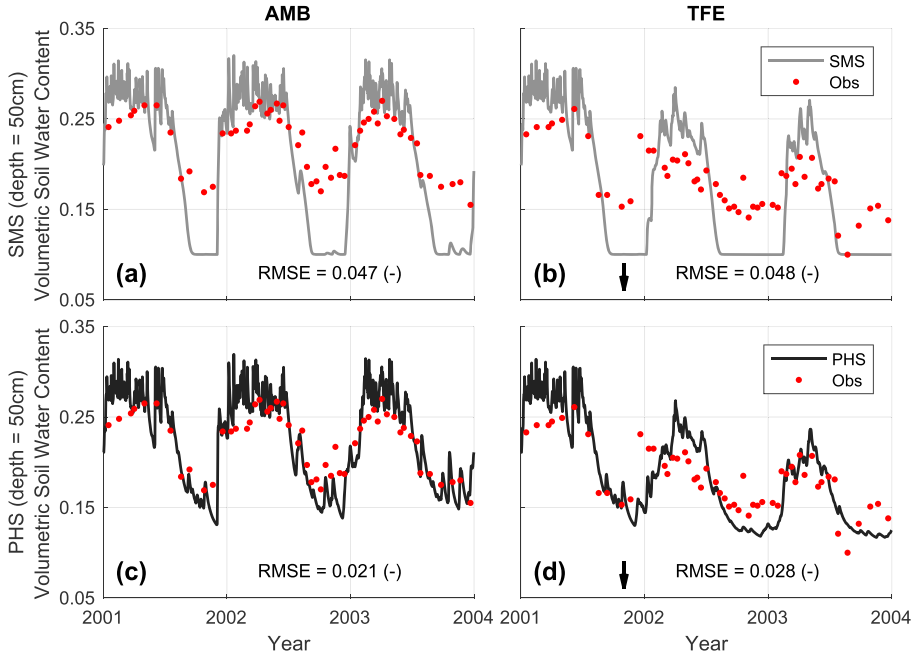

Figure 3. Volumetric soil water content (−) over time under ambient and TFE conditions at a depth of 50 cm. (a, b) SMS and (c, d) PHS. Arrows indicate start of TFE. Supporting information Figure S11 plots swven other soil depths. In the SMS configuration, soil moisture can tend to "stick" at water content of 0.1 during the dry season, which corresponds to $\psi_{soil} = -2.5$ MPa and is the value of the SMS soil wilting parameter, ψ_c. SMS = soil moisture stress; PHS = plant hydraulic stress; TFE = throughfall excluded; AMB = ambient precipitation throughfall; RMSE = root-mean-square error.

4.2. Vegetation Water Potential

PHS updates both the water stress and RWU parameterizations based on modeling vegetation water potential. Leaf water potential features a pronounced diurnal cycle, reaching −1.65 MPa at midday (Figure 4a). Most of the midday pressure drop occurs between ψ_{root} and ψ_{stem} ($\Delta = -1.47$ MPa), representing the root collar and upper stem, respectively. Stem, shade, and leaf curves are all roughly equal, resulting in overlapping lines in Figure 4a, relating to high stem-to-leaf conductance from the parameter values used in this experiment. Stem-to-leaf conductance does not drive leaf water potential in the current parameterization of the model but may be important to investigate further, given the reported dynamics of leaf conductance (Simonin et al., 2015).

Under TFE, model midday leaf water potential decreases to −2.31 MPa (Figure 4b). This change derives from a decrease in predawn root water potential (lower soil moisture) and in the drop in root water potential between predawn and midday (due to reduced soil-to-root conductance). This comports with previous evidence that seasonal changes in hydraulic resistance are larger belowground (Fisher et al., 2006). Despite reduced stem conductance, the pressure drop from root-to-stem acts in the opposite direction, reduced in magnitude to −1.02 MPa (from −1.47 MPa), following from 54% reductions in transpiration. In this way, stomatal regulation serves to mitigate the drop in leaf water potential due to soil drying and reduced hydraulic conductance.

Midday leaf water potential features a seasonal cycle, with lower values during the dry season (Figure 4c). Under ambient conditions, modeled root water potential values comport well with wet season observations in Fisher et al. (2006) but are less negative than dry season observations. Modeled leaf water potential values under ambient conditions are less negative than field observations (Fisher et al., 2006, report average ψ_{leaf} of −1.71 MPa during the wet season and −2.47 MPa during the dry season) but are within the range of observations. The parameter values used here may underestimate isohydricity (which would be reflected by minimal leaf water potential drop during drought) in response to TFE, given that observations showed no significant difference between ambient and TFE leaf water potential (Fisher et al., 2006).

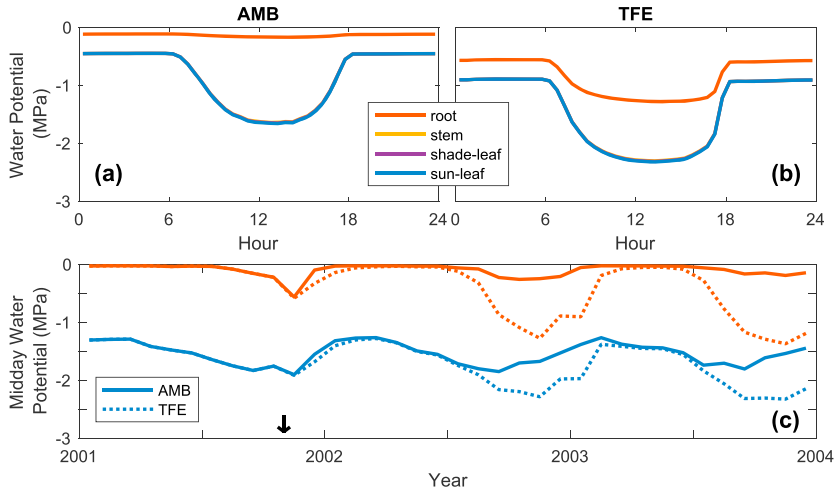

Figure 4. (a, b) The 2003 dry season (September-October-November) diurnal mean of modeled vegetation water potential under ambient and TFE conditions. Curves are drawn for sunlit leaf, shaded leaf, stem, and root water potentials, with the latter three overlapping. (c) Monthly mean midday (12–14 hr) vegetation water potential under ambient (solid line) and TFE (dotted line) conditions. Here curves are drawn only for sunlit leaf and root water potential. The arrow indicates the start of TFE. AMB = ambient precipitation throughfall; TFE = throughfall excluded.

4.3. Stress Dynamics

Modeling vegetation water potential enables a diurnal mode of variability in vegetation water stress. While the SMS stress factor has minimal diurnal variability, PHS features increased stress at midday (Figures 5a and 5b), corresponding to the drop in leaf water potential induced by increasing demand for transpiration (Figures 4b and 4c). Average midday stress values are comparable between the two model configurations during the 2003 dry season (Figure 5), but PHS achieves more photosynthesis over the course of the average dry season day (Figure S4), due to lower stress in the mornings and afternoons.

The SMS stress factor lacks diurnal variability, because it is based on average root zone soil matric potential (equation (3)), which evolves over longer timescales. PHS utilizes leaf water potential to calculate stress (equation (10)), which responds to both water supply and transpiration demand. As such, the PHS stress factor responds to both soil moisture and VPD, while SMS responds only to soil moisture (Figure 6). Under ambient conditions, SMS features significant stress associated with declining soil water status, but PHS stress is primarily demand driven, with less impact from soil moisture (Figures 6a and 6c). With TFE, stress

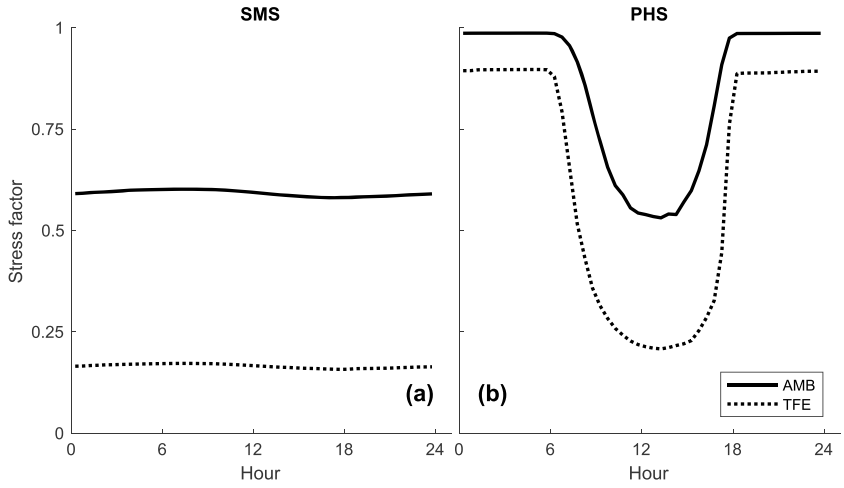

Figure 5. The 2003 dry season (September-October-November) diurnal mean water stress function for (a) SMS and (b) PHS. Note that the water stress factor equals 1 when there is no stress and 0 when fully stressed. SMS = soil moisture stress; PHS = plant hydraulic stress; AMB = ambient precipitation throughfall; TFE = throughfall excluded.

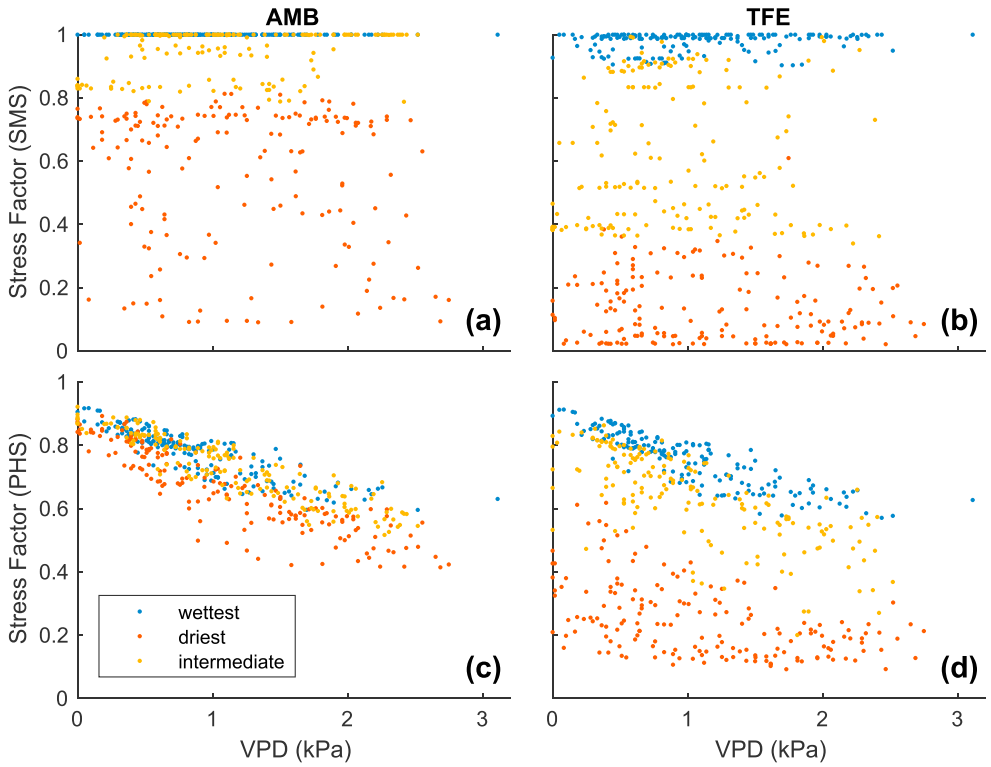

Figure 6. Water stress factor versus vapor pressure deficit (2002–2003), constrained to time steps with downwelling shortwave radiation between 400 and 425 W/m^2 ($n = 515$). Radiation is controlled to highlight the relationship with VPD, the reverse (controlling for VPD) is shown in supporting information Figure S6. For SMS (a, b), data are subdivided based on average soil matric potential, weighted by root fraction. For PHS (c, d), data are subdivided based on predawn (5 hr) root water potential. Blue dots represent the wettest tercile, yellow dots represent the intermediate tercile, and red dots represent the driest tercile (values defining each tercile are in Table 2). PHS utilizes leaf water potential as the basis for its water stress factor, which introduces a dependence on transpiration demand. AMB = ambient precipitation throughfall; TFE = throughfall excluded; VPD = vapor pressure deficit.

increases in both model configurations, and the effect of soil moisture on PHS stress increases markedly (Figure 6d).

4.4. GPP

The two stress parameterizations feature differing seasonal cycles of GPP, with PHS experiencing less seasonal variability in stress (Figures 7a–7d). Under ambient conditions, SMS predicts little to no stress (f_w = 1) during the wetter months (January through July). Meanwhile, PHS models significant stress, with highly variable f_w, ranging as low as 0.5. Despite abundant soil water, PHS still imposes stress, due to high transpiration demand when VPD and downwelling solar radiation are high. This results in lower wet season GPP and lower GPP variability than with SMS (Figures 7e and 7g). Contrastingly, SMS imposes more stress than PHS during the dry season (Figures 7b and 7d), resulting in lower dry season GPP. Observations show that GPP increases at Caxiuanã during the dry season (Restrepo-Coupe et al., 2017), suggesting that both model configurations, but especially SMS, may overestimate dry season water stress under ambient conditions.

The modeled effect of TFE is relatively small during the wet season, with modeled reductions in GPP of 1.3% and 3.8% for PHS and SMS, respectively. Based on transpiration observations, both configurations likely underestimate the TFE effect during the wet season (discussed further in section 5.2). SMS imposes more dry season stress, resulting in a 63% reduction of GPP due to TFE, compared to 44% with PHS. Comparing dry season stress to the wet season, and TFE conditions to ambient, precipitation shortfalls (and the associate reductions in soil moisture) lead to less added stress under PHS as compared to SMS. However, PHS experiences more stress overall, due to the effects of xylem tension imposed by the gradient of water potential from soil-to-leaf (discussed further in section 5.2). The sensitivity of leaf gas exchange to transpiration

Table 2
Root Zone Soil Potential[a](MPa) Terciles

Simulation	T1	T2
SMS, Ambient	−0.01	−0.54
SMS, TFE	−0.29	−1.74
PHS, Ambient	−0.01	−0.05
PHS, TFE	−0.05	−0.33

Note. The two cut points are used to divide the points in each subplot of Figure 6 into three groups, based on root zone soil moisture. SMS = soil moisture stress; PHS = plant hydraulic stress.
[a]SMS values correspond to daily mean root fraction weighted soil potential. PHS values correspond to predawn root water potential.

demand is subject to the representation of hydraulic conductance in PHS, which requires caveats related to parametric uncertainty and hydraulic simplifications (see section 2.5.4).

4.5. RWU

In addition to updating water stress, PHS implements updated RWU, consistent with hydraulic theory (Cai et al., 2018; Warren et al., 2015). The parameterization of RWU affects the vertical distribution of soil water (Figures 8 and S9), as SMS tends to achieve drier upper soil layers, whereas PHS spreads the drying effects of transpiration over a larger vertical extent. As described in section 4.1.3 (Figure 3), this yields a dry bias relative to soil moisture observations in the root zone for SMS (within the dry season).

RWU, within a given soil layer, is the product of hydraulic conductance ($k_{s,r}$) for water flow and the gradient ($\Delta\psi$) in water potential from $\psi_{\text{soil,i}}$ to ψ_{root} (see section 2.5.4). With PHS, reductions in RWU with drying are imposed by declining $k_{s,r}$, which decreases by almost 3 orders of magnitude as soil potential declines from 0 to −1 MPa (soil layer 5, Figure S7). This derives primarily from the exponential dynamics of soil conductivity (Brooks & Corey, 1964). $\Delta\psi$ tends to increase with drying (due to dynamic ψ_{root}), partially mitigating the reductions to RWU imposed by $k_{s,r}$. With SMS, the opposite is true: Reductions in RWU are imposed by declining $\Delta\psi$ and are (to a small extent) mitigated by increases in the (implied) conductance. RWU (within a given soil layer) is more sensitive to soil potential with PHS (Figure S10), which prevents soil potential from getting much lower than −1 MPa, as compared to values as low as −2.5 MPa under SMS.

While RWU within a given soil layer is more sensitive to soil potential with PHS, transpiration overall is less sensitive to shortfalls in precipitation associated with dry season onset and TFE (as compared to SMS, Figure S3). This is because, within PHS, there is more flexibility to compensate for dry layers by switching the RWU

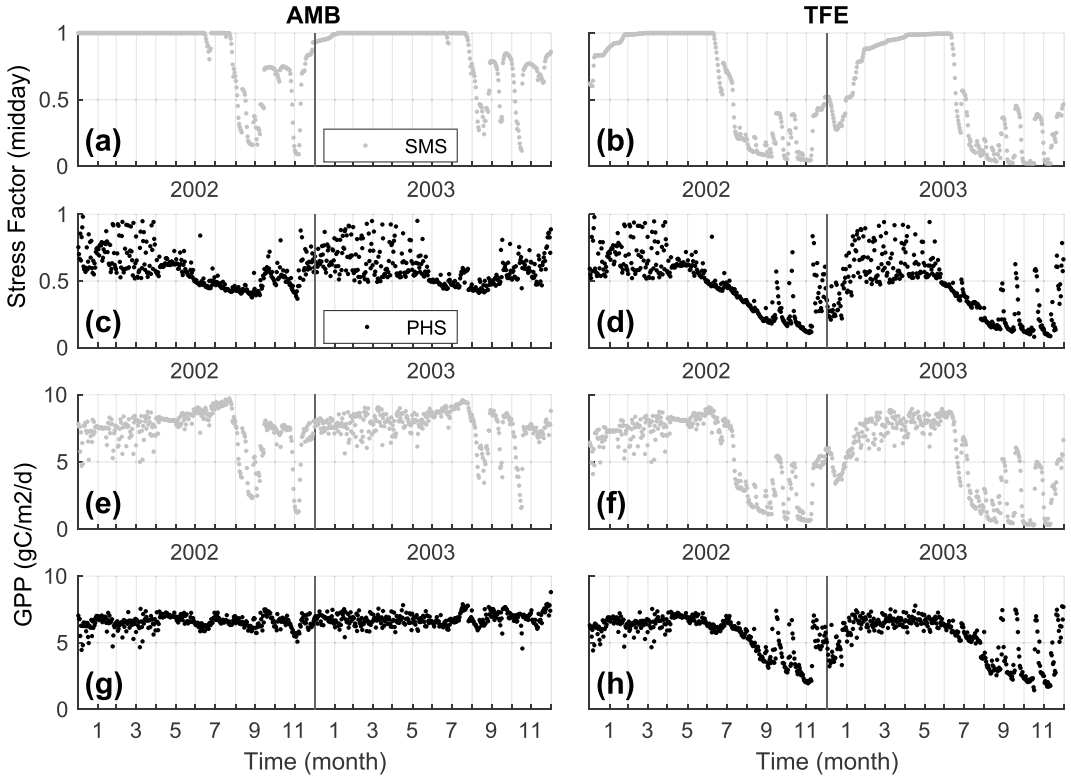

Figure 7. (a–d) Daily stress factor (midday, averaged over 12–14 hr) and (e–h) GPP (daily total) over 2002–2003 under ambient (left column) and TFE (right column) conditions. Output from the SMS configuration (a, b, e, and f) are plotted with gray color, while output from the PHS configuration (c, d, g, and h) are plotted in black. AMB = ambient precipitation throughfall; TFE = throughfall excluded; SMS = soil moisture stress; PHS = plant hydraulic stress.

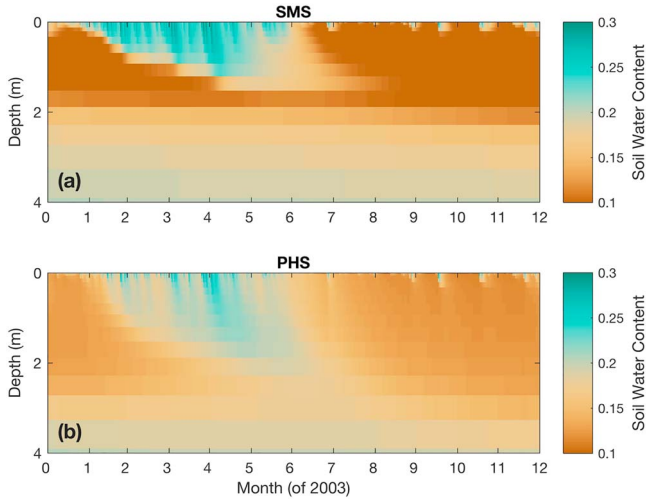

Figure 8. Vertical profile of soil water content (by volume) over 2003 under 60% throughfall exclusion, for (a) SMS and (b) PHS. Soil water content under ambient conditions is shown in supporting information Figure S9. PHS spreads the vegetation transpiration sink over a larger vertical extent, which prevents the very low soil moisture values observed in SMS. PHS = plant hydraulic stress; SMS = soil moisture stress.

to moist layers. As such, PHS can compensate for its sensitivity to soil potential by spreading the drying associated with the transpiration sink over a larger vertical extent (Figure 8). Following from this, with PHS, dry season transpiration is less sensitive to TFE, due to increased RWU from below 2 m in depth (Figure 9d). The shifting of water extraction based on water availability is also present under ambient conditions, as PHS shifts RWU from near-surface (0- to 0.2-m depth) to the deeper soil layers (beyond 0.2 m) during drydowns (Figures 9a–9c).

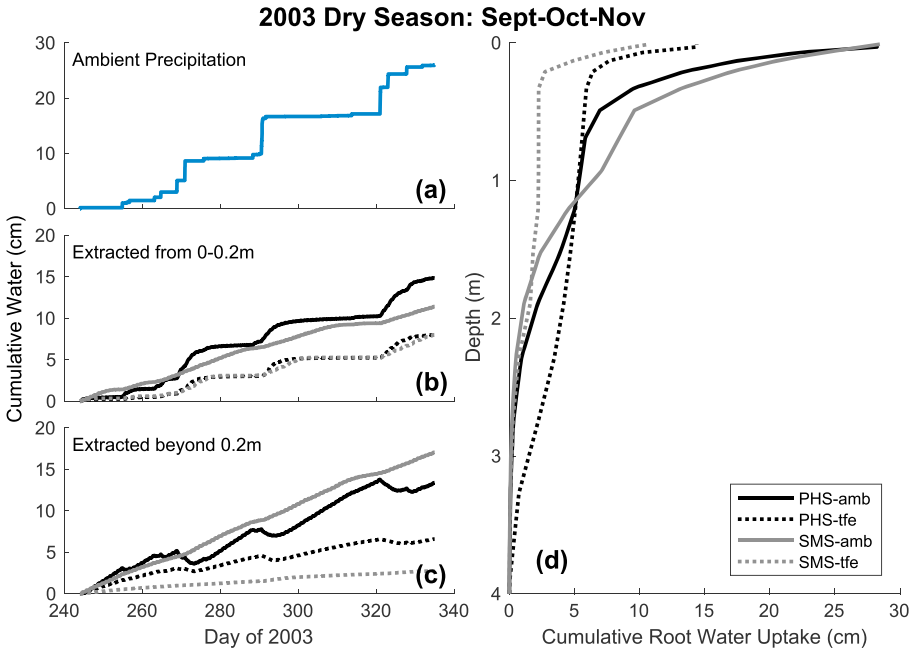

Figure 9. The 2003 dry season (September-October-November) cumulative root water uptake and precipitation. (a) Cumulative precipitation over time under ambient conditions (b, c) Cumulative water uptake over time from above and below 0.2 m, respectively. (d) Cumulative root water uptake over the soil column (accumulating from depth). An equivalent plot for the wet season is shown in supporting information Figure S5. The new root water uptake parameterization allows PHS to maintain more transpiration under throughfall excluded by utilizing more deep soil water. SMS = soil moisture stress; PHS = plant hydraulic stress.

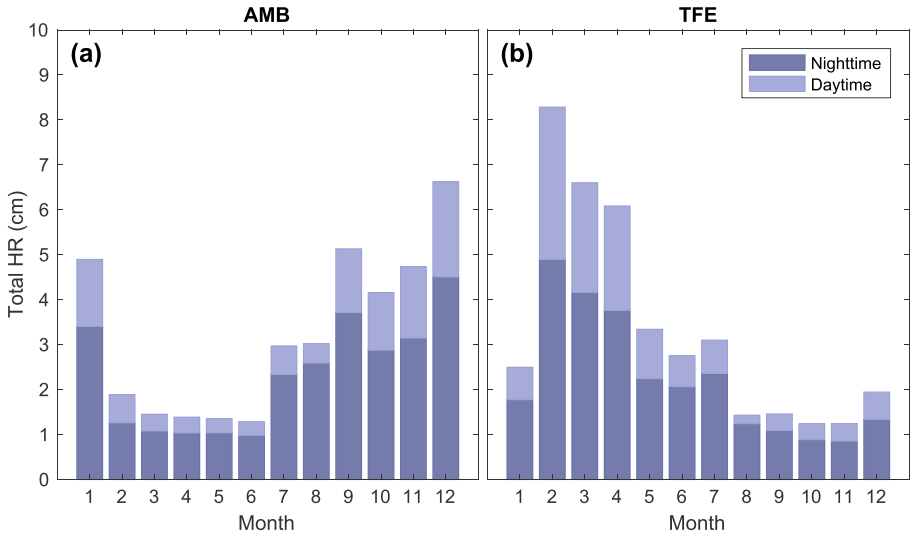

Figure 10. Total hydraulic redistribution (cm) by month across 2003. For (a) ambient throughfall conditions and (b) 60% throughfall exclusion. Darker shading shows portion of HR)at night [6 p.m., 6 a.m.), lighter shading shows portion of HR during the day [6 a.m., 6 p.m.). Total HR refers to the sum of all negative root water uptake flows, whenever water is deposited by roots into a given soil layer (instead of being extracted). HR = hydraulic redistribution; AMB = ambient precipitation throughfall; TFE = throughfall excluded.

Lastly, PHS eschews constraints on RWU imposed by SMS (equation (7)), which sets extraction to 0 if $\psi_{soil,i}$ is drier than ψ_c and to a maximal value when $\psi_{soil,i}$ is wetter than ψ_o (SMS parameters for soil potential with stomates fully closed and open, respectively). Hydraulic theory does not support either constraint. Furthermore, the nonlinearity of RWU at ψ_c (Figure S7) creates a situation where dry soil layers tend to stick at $\psi_{soil,i}=\psi_c$ (Figure 3). Likewise, the constraint at ψ_c precludes the representation of HR.

4.6. HR

SMS precludes HR (contrary to PHS) setting RWU to zero when reversed gradients in water potential occur ($\psi_{soil,i}<\psi_c$). With PHS, HR totals to 38.9 cm under ambient conditions and 40.0 cm under TFE over the course of 2003, with the majority (28.0, 26.7 cm) of this HR occurring at night (Figure 10), in line with established theory (Jackson et al., 2000; Lee et al., 2005) and observations (Burgess et al., 1998; Oliveira et al., 2005). HR occurs in both directions (Figure S8) but is predominately downward (AMB: 30.7 cm, TFE: 33.8 cm). The amount of HR is difficult to evaluate due to scarce observations. The simplicity of the hydraulic representation may lead to overestimating HR, which is discussed further in section 5.3.4.

4.7. Soil Moisture Effect on Transpiration

Model soil potential shows limited relationship to sap flux observations under ambient conditions (Figures S12b and S12f), which is indicative of limited SMS. However, in the SMS configuration, modeled transpiration decreases strongly with more negative soil potential (Figure S12a), biasing the model relative to observations (Figure 11a).

Sap flux observations under TFE show a stronger relationship with soil potential especially with PHS (Figures S12h and S12d). With SMS, the modeled attenuation of transpiration with soil potential again seems to bias modeled transpiration (Figure 11b). The two PHS simulations feature less structure in transpiration bias versus soil potential and less bias overall (Figures 11c and 11d).

5. Discussion

5.1. Can Modeling Vegetation Water Potential Improve the CLM?

In this study, we have implemented plant hydraulic theory within CLM5, using dynamic vegetation water potential to modulate leaf gas exchange and RWU. Darcy's law, which is already used to model soil water movement in the CLM, offers a useful approximation for vegetation water fluxes (Sperry et al., 1998). PHS installs a model for predicting vegetation water potential by extending Darcy's law through the vegetation substrate (Figure 1), creating four new water potential prognostic variables (ψ_{root}, ψ_{stem}, $\psi_{shade\text{-}leaf}$, and $\psi_{sun\text{-}leaf}$). The model is able to capture expected diurnal and seasonal dynamics of vegetation water poten-

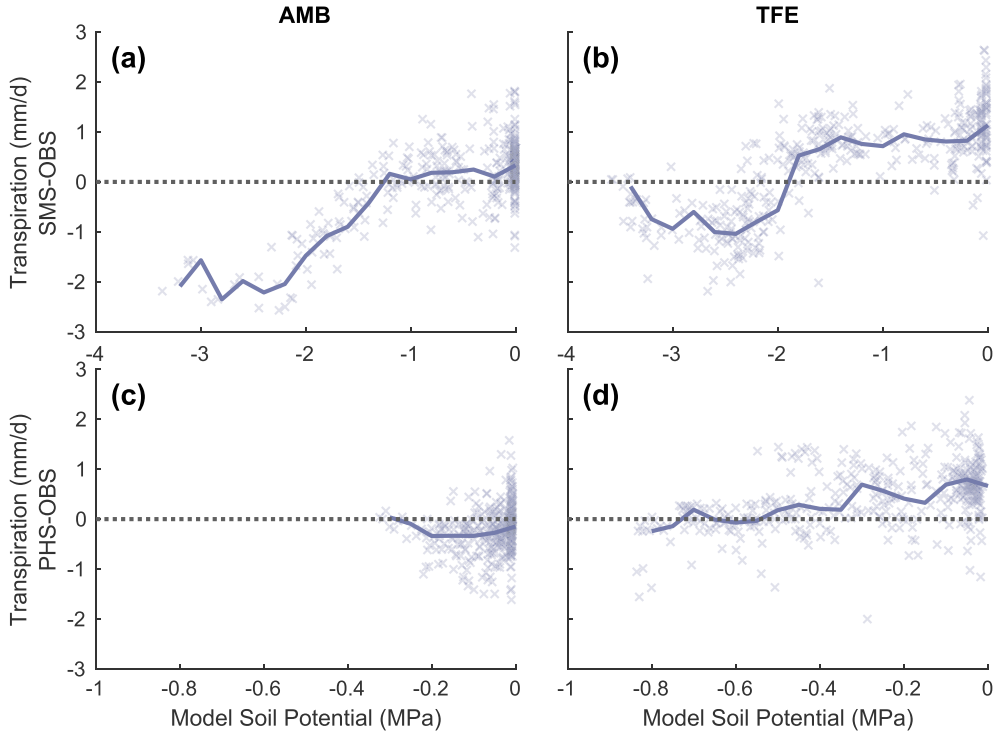

Figure 11. Difference between modeled and observed transpiration (mm/day) versus model soil potential (MPa), for (a, b) SMS and (c, d) PHS. Solid lines are drawn at the median, binning points every 0.2 MPa for SMS and 0.05 MPa for PHS (note the different soil potential axes). Dotted lines are drawn at zero, where modeled and observed transpiration are in agreement. The two models use different root water uptake paradigms, from which we define different operators for column effective soil potential. For SMS we average over the soil column weighted by root fraction and over time (daily mean). For PHS we use predawn (5 hr) root water potential. Based on available observations, $n = 414/436$ days under ambient/TFE conditions. AMB = ambient precipitation throughfall; TFE = throughfall excluded; PHS = plant hydraulic stress.

tial, with lower values within the stem and leaves at midday and during the dry season (Figure 4). PHS uses the new vegetation water potential variables to advance the physical basis for representing the SPAC, particularly with regard to modeling vegetation water stress and RWU.

To demonstrate the new model dynamics, we utilized a site-level experiment testing PHS by simulating the Caxiuanã throughfall exclusion experiment (Fisher et al., 2007). We found that PHS improves output for both transpiration and soil moisture relative to observations as compared to the control model (see section 4.1 and Figures 2 and 3). While this is encouraging, especially given the soil moisture dependence of the SMS bias (see section 4.7), the improvement is specific to the site and experiment described herein, and model skill will need to be reevaluated in a broader context. Instead, the value of opting for a single site (in lieu of global simulations) resides in the opportunity to perform detailed analyses to elucidate the new model dynamics in order to complement this first description of PHS.

5.2. Stomatal Conductance: SMS Versus Xylem Tension Stress

The first of these analyses is of the response of stomatal conductance stress to environmental factors, namely, soil moisture, VPD, and solar radiation. The Medlyn stomatal conductance model, as implemented in the CLM, requires a notion of water stress to attenuate stomatal conductance in order to capture the effects of diminishing water supply, with various relevant implementations described in the literature (see section 2.3). We tested two such approaches, which alternatively base stress on either soil water potential (SMS) or leaf water potential (PHS). The two configurations feature significantly different stress dynamics on both diurnal and seasonal timescales (Figures 5 and 7).

Leaf water potential is (in simplified terms) the sum of soil water potential and the gradient of water potential from soil-to-leaf ($\psi_l = \psi_s + \Delta\psi$). Therefore, using ψ_l as the driver of water stress preserves a relationship between stress and soil potential but now also represents the effect of increasing demand for transpiration

(reflected by increases in $\Delta\psi$). PHS offers a mechanistic approach to water stress, utilizing a physical justification that interprets water stress as the result of increasing xylem tension, which has previously been used as a primary (Sperry et al., 2017) or contributing (Novick et al., 2016) factor to stomatal regulation. In the model, vegetation will (according to the specific hydraulic parameter values) limit transpiration in order to avoid overly negative leaf water potential values, which are associated with cavitation and embolism (Tyree & Sperry, 1989). As a result, PHS stress responds to changing soil moisture and, unlike SMS, also responds to VPD and downwelling solar radiation (Figure 6), which modulate transpiration demand. This imparts a diurnal pattern to PHS stress, with higher stress around midday, whereas with SMS, stress is relatively constant throughout the day (Figure 5). The PHS stress formulation will impart an increased sensitivity of GPP to rising VPD under climate change, which could lead to a diminished terrestrial carbon sink relative to SMS projections.

Soil water potential approaches (as in SMS) lack a straightforward physical basis but rather empirically relate stomatal conductance and/or photosynthetic parameters with soil potential (or soil moisture). However, in the case of SMS, the empirical relationship is very difficult to constrain, due to scarce observations of the stress driver, root-fraction-weighted soil potential. As a result, SMS functions have been shown to contribute significant uncertainty to the carbon cycle in ESMs (Trugman et al., 2018). Leaf water potential, on the other hand, is more easily measured in situ (Boyer, 1967) and has been shown to correlate with remote sensing products (Momen et al., 2017), offering better observational constraints for PHS. Likewise, incorporating plant hydraulics may allow for improved model representation of tree mortality (McDowell et al., 2018). The PHS formulation represents an incremental approach to coupling stomatal conductance to leaf water potential, inheriting the established CLM stomatal conductance model (Franks et al., 2018), while adapting the water stress factor to depend on leaf water potential. This could be refined in future versions of PHS, incorporating recent work that directly incorporates leaf water potential within the stomatal optimization (Anderegg, Wolf, et al., 2018; Sperry et al., 2017; Wolf et al., 2016).

5.3. Structural Improvements in Modeling RWU

5.3.1. Dynamic Vegetation Water Potential

PHS introduces dynamic vegetation water potential (Figure 4), for the first time, into the default configuration of the CLM. Seasonally and diurnally dynamic leaf water potentials are observed in the field (Fisher et al., 2006), adjusting to variations in soil water supply and transpiration demand. Dynamism in the gradient of water potential from soil-to-leaf, according to the Darcy's law approximation of vegetation water fluxes, drives RWU. This is especially important for partitioning the transpiration sink among soil layers with varying soil potential states (Jarvis, 2011). A mechanistic representation of RWU with dynamic vegetation water potential allows for modeling a range of water use strategies and/or testing hypotheses regarding such strategies on the ESM scale. One example is testing the effects of increasing carbon allocation to root biomass, which was not well represented in previous versions of the CLM, because water availability depended on relative root fraction and would not respond to increase in absolute biomass. Another example is testing the effects of iso/anisohydry, which can be diagnosed from remote sensing observations (Konings & Gentine, 2017), on leaf gas exchange and drought vulnerability. The spectrum of isohydric to anisohydric behavior, corresponding to highly regulated versus relatively unregulated leaf water potential, cannot be represented in previous versions of the model that do not model leaf water potential. Likewise, variation in HSM, which have been shown to correlate with drought sensitivity (Anderegg, Konings, et al., 2018), can now be represented in the model due to prognostic leaf water potential.

5.3.2. Mechanistic Hydraulic Conductance, With Response to Drying

Likewise, PHS implements mechanistic hydraulic conductance through the SPAC, reflecting declines in conductance associated with decreasing water potential in both plant vessels and soil substrate (Tyree & Sperry, 1989). Hydraulic theory describes soil conductance as featuring an exponential relationship with soil potential (Brooks & Corey, 1964), ranging 3 orders of magnitude over the range of soil potential observed in our simulations (Figure S7). This shapes the PHS response of RWU to soil drought and is not captured by the linear loss of RWU exhibited in SMS (between the parameters: ψ_o and ψ_c, Figure S10). As a result, PHS RWU is more sensitive to drying soils, which seems to ameliorate dry biases in soil moisture observed in SMS relative to observations (Figure 3). At the same time, the mechanistic approach of PHS better reflects soil-root hydraulic theory (Cai et al., 2018; Warren et al., 2015).

5.3.3. Compensatory RWU

Utilizing a hydraulic approach (with dynamic vegetation water potential and mechanistic hydraulic conductance) enables a more flexible representation of RWU. This includes the ability to model HR (next section) and compensatory RWU. Compensatory RWU occurs when soil water extraction switches soil layers to maintain transpiration through precipitation shortfalls. For example, as surface soil layers dry, tap roots can be used to harness reserves of soil water at depth (Oliveira et al., 2005), partially compensating for reduced RWU near the surface. In an SMS-style paradigm, this process is not fully represented.

With identical rooting profiles, PHS extracts 29% of transpiration from beyond 2-m depth under TFE (during the 2003 dry season) as compared to 13% with SMS. In PHS, as the surface soil layers dry out, conductance decreases rapidly, leading to reduced near-surface RWU. In response, the vegetation "pulls" harder, as ψ_{root} becomes more negative, creating a larger gradient to the deeper soil layers, yielding increased RWU in those still-moist layers. SMS lacks the flexibility to achieve this type of compensatory RWU, because it models RWU fluxes based on a constant soil wilting potential (ψ_c) and does not explicitly impose a loss of hydraulic conductance as soils dry. As a result, PHS maintains higher levels of transpiration and photosynthesis than SMS during the dry season under both ambient and TFE conditions (Figures S3 and 7). This process may be especially important for modeling evapotranspiration in semiarid ecosystems (Jarvis, 2011) and in Amazonia, where water contributions of deep roots are often important (Nepstad et al., 1994).

5.3.4. HR

PHS simulates substantial HR at our test site, both upward and downward (Figures 10 and S8), which conforms with field observations (Burgess et al., 1998; Oliveira et al., 2005). Modeled HR is weighted toward downward transfers, moving near-surface water from rain events deeper into the soil column. This may serve to save excess water it for when it is most needed, such as during the dry season, and would seem to convey an advantage to deep-rooted individuals, banking water for later use out of reach of shallow-rooted competitors. HR can offer significant water subsidies during dry periods (Jackson et al., 2000) and has been highlighted as an important missing feature in CLM (Lee et al., 2005; Tang et al., 2015). However, we should note that observations of HR are extremely difficult and rare, and the degree to which HR actually occurs in real-world systems remains unclear. Unequivocal detection of HR involves the observation of reverse flow along transport roots, typically at rates close to the detection threshold of sap flow monitoring systems.

Installing a representation of HR was not a primary objective in the development of PHS. Rather, it was the natural consequence of our simplified Darcy's law implementation for RWU. However, it remains to be seen whether HR, as modeled in this implementation, is a feature or a liability. One challenge we faced was that in an initial implementation of PHS, HR seemed to oversupply the top layer of the soil column (spanning 0 to 2 cm below the ground surface) and thus significantly degraded modeled soil evaporation (not shown). To remedy this problem, we set the hydraulic conductance to zero in the uppermost soil layer, disallowing any RWU there.

PHS may overestimate HR, given the simplified root system architecture (Bouda & Saiers, 2017) and the lack of an explicit representation of fine-root cavitation (Kotowska et al., 2015). In our simulations, HR increases annual total RWU by up to 52% relative to transpiration alone (2003, TFE). Other models, similar to the SMS paradigm, disallow HR by constraining RWU to be positive (Xu et al., 2016). We view the PHS implementation of HR into the default versions of the CLM as a "null" hypothesis for the functioning of this process and as a platform to allow further refinement from the plant hydraulics community. Isotopologues of water could be used as a tool to further constrain this redistribution in the CLM in the future.

5.4. The Influence of Soil Moisture on Transpiration

The stress effects of declining soil water potential seems to bias SMS predictions of transpiration relative to sap flux observations (Figures 11a and 11b). Under ambient conditions, soil water shows little relationship with sap flux observations with either model configuration (Figures S12b and S12f); however, SMS modeled transpiration decreases strongly in response to soil drying (Figure S12a). This creates a bias where SMS underestimates transpiration during the drier soil conditions, which is in line with Bonan et al. (2014), where the water stress factor was found to impose too much attenuation of transpiration (in CLM4.5).

With PHS the transpiration bias does not seem to strongly depend on soil potential while also featuring less bias overall (Figures 11c and 11d). Likewise, PHS yields a stronger relationship than SMS between soil potential and sap flux observations during TFE (Figures S12d and S12h). While improvements modeling transpiration were expected with PHS (more parameters), it seems promising that the gains are associated

with the reduction of a soil moisture induced bias. This could indicate that PHS better models the relationship between soil potential and water stress or the dynamics of soil potential itself (or a combination thereof). The reduction in bias introduced by the water stress function (especially as it depends on soil potential) represents a major development, given repeated calls to improve vegetation water stress in the next generation of terrestrial biosphere models (Powell et al., 2013; Rogers et al., 2017; Trugman et al., 2018).

5.5. Benefits and Limitations of PHS

5.5.1. Benefits

1. Advances the physical basis of the CLM
   - Mechanistic xylem tension stress replaces empirical SMS
   - RWU reflects established hydraulic theory
   - More appropriate response of water availability to root abundance
2. Improves modeled vegetation hydrodynamics
   - Better match to observations of soil moisture and transpiration (higher correlation, lower RMSE)
   - Importantly, the improvements modeling transpiration are achieved by removing a bias associated with soil water status
   - Permits representation of compensatory RWU and HR
   - Avoids excessive soil layer drying observed with SMS
3. Creates an interface to new observational constraints
   - Parameters are better represented in trait databases (e.g., k_{max}, p_{50}).
   - New state variables modeling vegetation water potential are introduced, which are measured in situ and have been shown to correlate with remote sensing products (Momen et al., 2017).
   - And given that vegetation water potential is downstream of soil water potential, this may actually provide an important constraint on root zone soil moisture.
4. Enables a platform for testing various hydraulics-oriented hypotheses within the ESM context
   - What are the relative contributions to water stress of VPD versus soil moisture?
   - Does the spectrum of isohydric versus anisohydric regulation of vegetation water potential explain patterns in the terrestrial carbon and hydrological cycles?
   - Are certain regions of the concatenated hydraulic parameter/climate space particularly vulnerable to climate change?

5.5.2. Limitations

1. Plant hydraulics are highly simplified.
   - Does not model vegetation tissue water storage (capacitance)
   - Loss of conductance (vulnerability) not integrated across vegetation tissue or soil matrix (based on lower terminus)
   - Stem-to-leaf resistance is not fully deployed
   - Simplified root system architecture
   - These simplifications create a null hypothesis for further testing by the hydraulic community and yield a relatively light-weight model
2. Uncertainty regarding the parameterization of water stress
   - PHS models water stress (f_w) as a sigmoidal function of leaf water potential, which is used to attenuate V_{cmax}
   - Stress attenuation of V_{cmax} was also utilized in CLM4.5/SMS, which allowed for easier comparison between model versions
   - However, significant uncertainty exists in coupling the PHS water stress factor to the Medlyn stomatal conductance model, which could be resolved in future versions by recent work that directly incorporates hydraulic limitations within the stomatal optimization (Anderegg, Wolf, et al., 2018; Sperry et al., 2017; Wolf et al., 2016).
3. Increased model complexity
   - Can potentially be mitigated by hydraulic trait coordination, improved parameter priors, and observational constraints on vegetation water potential
   - However, the spatial scale of the CLM does not match to the experiments associated with reported parameter values in trait database
4. We do not provide a definitive assessment on model skill.
   - Single site

- Results specific to experimental setup and parameter values
- However, this allows for more detailed analysis of the model dynamics to supplement the model description

6. Conclusion

The PHS configuration of the CLM5 within the Community Earth System Model (CESM2) is, to our knowledge, the first land surface model within an ESM with a representation of vegetation water potential running in its default configuration. In this paper, we have described the model implementation and illustrated a comparison of the model dynamics for a tropical rainforest site subjected to water limitation, given that prediction of rainforest responses to drought is one of the key uncertainties in the ESM predictions (Huntingford et al., 2013).

Overall, the new model behavior differs from the default configuration in ways that are expected, given its structural properties, and, in many cases, provides better correspondence with observations than the default structure. Modeling vegetation water potential allows for new parameterizations for the model representations of RWU and vegetation water stress, which better conform to established plant hydraulic theory. PHS RWU, driven by dynamic vegetation water potential, allows representation of compensatory RWU and HR. As a result, PHS utilizes more of the soil column to buffer precipitation shortfalls, which, in both the ambient and TFE simulations, reduces dry season biases in transpiration and root zone soil moisture. PHS water stress requires vegetation to avoid extreme values of leaf water potential, associated with excessive xylem tension and hydraulic failure. This incorporates a dependence of the CLM water stress factor on transpiration demand, which was previously not represented. As a result, photosynthesis is more sensitive to VPD with PHS.

The new model structure will likely have significant implications on climate feedbacks, given the changes in precipitation and VPD sensitivity introduced by PHS. In this paper, however, we have not aimed at undertaking a comprehensive assessment of which model structure performs better, given the substantial parametric uncertainty in both models, and the dependence on numerous other features of the CLM external to water stress representation that contribute to model-observation divergences, such as, in this case, the overestimation of wet season transpiration under TFE.

In lieu of this type of assessment, we propose that the new PHS model structure (1) is more closely aligned with known plant hydraulics theory, (2) provides significantly improved connections to real-world observational data streams (of leaf and stem water status, sap flow, and percent loss conductance), and (3) represents known features of ecohydrological function that the control model cannot capture, including HR, changes in the depth of water uptake with drought stress, plant embolism impacts on gas exchange, and responses of water uptake to changes in root abundance.

Appendix A: Appendix to Model Description

A1. Details of Water Supply

PHS resolves flow across four different segments, soil-to-root, root-to-stem, stem-to-leaf, and leaf-to-transpiration.

Stem-to-leaf. The area bases are sunlit and shaded leaf area, respectively. Note that gravity is assumed negligible here. Likewise, there is no length scaling applied to maximum conductance. Therefore the input parameter for $k_{\text{leaf,max}}$ should be a conductance (s^{-1}).

$$\begin{aligned} q_{\text{sun}} &= k_{\text{sun}} \cdot \text{LAI-sun} \cdot \left(\psi_{\text{stem}} - \psi_{\text{sun-leaf}}\right) \\ q_{\text{shade}} &= k_{\text{shade}} \cdot \text{LAI-shade} \cdot \left(\psi_{\text{stem}} - \psi_{\text{shade-leaf}}\right) \end{aligned} \tag{A1}$$

$$k_{\text{sun}} = k_{\text{shade}} = k_{\text{leaf,max}} \cdot f\left(\psi_{\text{stem}}\right) \tag{A2}$$

$$f(\psi) = 2^{-\left(\frac{\psi}{P50}\right)^{c_k}} \tag{A3}$$

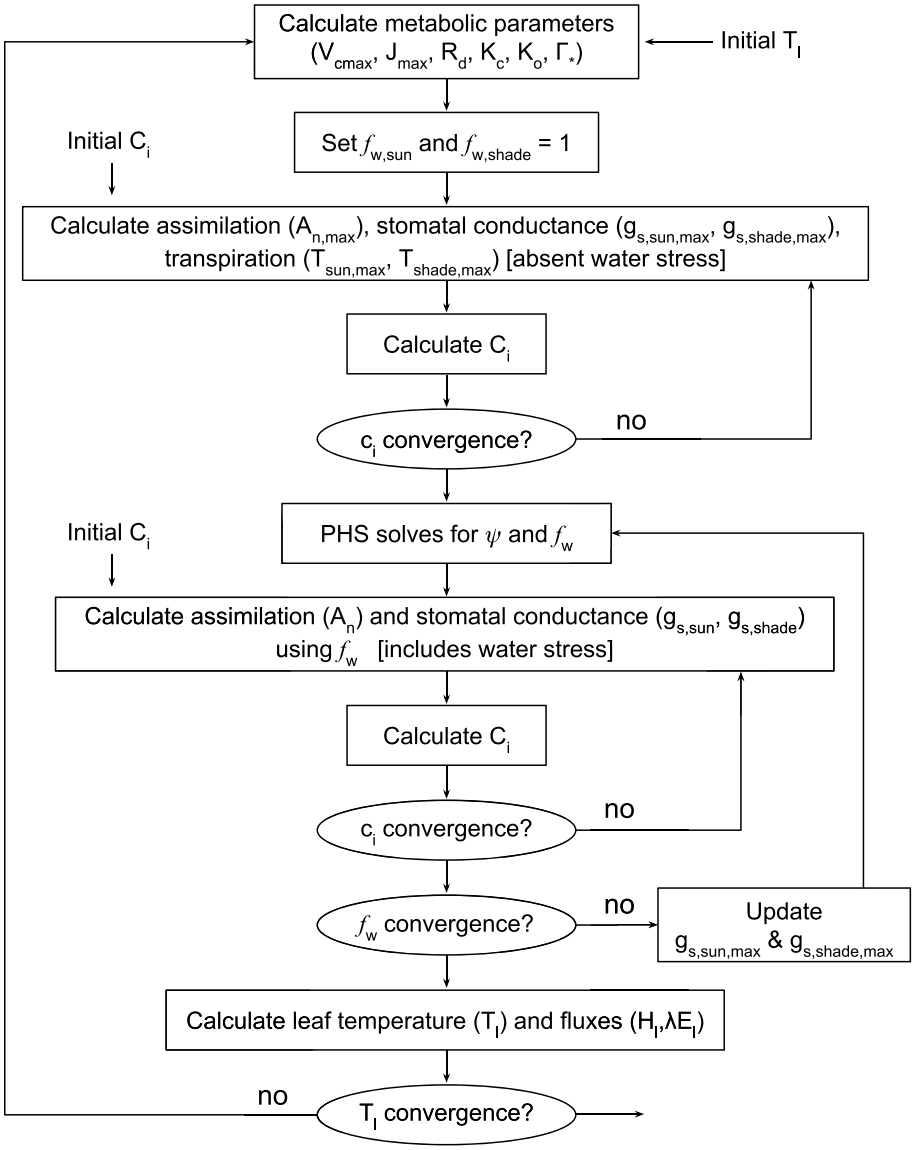

Figure A1. Flow chart of plant hydraulic stress (PHS) iterative solution.

Root-to-stem. The area basis is stem area index. The input parameter is maximum stem xylem conductivity ($K_{\text{stem,max}}$). Stem conductance (k_{stem}) is the result of scaling maximum conductivity by the tree height (h) and applying loss relative to maximum conductance via the vulnerability curve $f\left(\psi_{\text{root}}\right)$.

$$q_{\text{stem}} = k_{\text{stem}} \cdot \text{SAI} \cdot \left(\psi_{\text{root}} - \psi_{\text{stem}} - \rho g h\right) \tag{A4}$$

$$k_{\text{stem}} = \frac{K_{\text{stem,max}}}{h} \cdot f\left(\psi_{\text{root}}\right) \tag{A5}$$

Soil-to-root. Area basis is RAI in soil layer i, which is based on the layer root fraction times the total root area. Total root area is calculated as the sum of stem and leaf area indices multiplied by a relative root area parameter (f_{root}). The vertical root distribution is defined by the layer root fraction (r_i), which follows a one-parameter (by plant functional type) power law decay following Jackson et al. (1996).

$$q_{\text{sr},i} = k_{\text{sr},i} \cdot \text{RAI}_i \cdot \left(\psi_{\text{soil,i}} - \psi_{\text{root}} - \rho g z_i\right) \tag{A6}$$

$$\text{RAI}_i = f_{\text{root}} \cdot (\text{SAI} + \text{LAI}) \cdot r_i \tag{A7}$$

$$k_{\mathrm{sr},i} = \frac{k_{r,i} + k_{s,i}}{k_{r,i} \cdot k_{s,i}} \tag{A8}$$

$$k_{r,i} = \frac{K_{r,\max}}{l_i} f\left(\psi_{\mathrm{soil,i}}\right) \tag{A9}$$

$$l_i = z_i + x \tag{A10}$$

$$k_{s,i} = \frac{K_{s,i}}{d} \tag{A11}$$

The soil-and-root conductance $k_{\mathrm{sr},i}$ reflects two resistors in series, from soil-to-root ($k_{s,i}$) and through the root tissue ($k_{r,i}$). The root tissue conductance is attenuated via the vulnerability curve framework. The input parameter is maximum root xylem conductivity, on the basis of RAI as defined above. The root conductivity is scaled by the conducting length, which is estimated as the sum of soil layer depth (z_i) and average lateral extent (x, static parameter). The soil conductivity $K_{s,i}$ is calculated from the layer soil matric potential ($\psi_{\mathrm{soil},i}$) and soil properties as described in Oleson et al. (2013) utilizing typical soil hydraulic theory (Brooks & Corey, 1964; Clapp & Hornberger, 1978). The soil conductance ($k_{s,i}$) is the result of scaling the conductivity by d, the distance between roots estimated following M. Williams et al. (1996) and Bonan et al. (2014).

A2. Details of Water Demand

The CLM5 implementation utilizes the Medlyn stomatal conductance model (Medlyn et al., 2011) while also applying water stress through V_{cmax}. Transpiration is calculated reflecting contributions from both stomatal conductance and leaf boundary layer conductance (g_b).

$$V_{\mathrm{cmax}} = f_w V_{\mathrm{cmax,ww}} \tag{A12}$$

$$g_s = g_0 + \left(1 + \frac{g_1}{\sqrt{D}}\right)\frac{A}{C_a} \tag{A13}$$

$$\begin{aligned} E_{\mathrm{sun}} &= g_{s,\mathrm{sun}} * \rho * \mathrm{VPD} * lai_{\mathrm{sun}} * \left(1 + \frac{g_{s,\mathrm{sun}}}{g_b}\right)^{-1} \\ E_{\mathrm{shade}} &= g_{s,\mathrm{shade}} * \rho * \mathrm{VPD} * lai_{\mathrm{shade}} * \left(1 + \frac{g_{s,\mathrm{shade}}}{g_b}\right)^{-1} \end{aligned} \tag{A14}$$

At the beginning of a set of PHS iterations, we solve for $E_{\mathrm{sun,max}}$ and $E_{\mathrm{shade,max}}$, by running the stomatal conductance scheme with f_w set to 1 (no stress). Within each PHS iteration, we do not resolve the full stomatal conductance scheme but instead consider only the linear attenuation of stomatal conductance by f_w. Transpiration is attenuated relative to the maximal values according to leaf water potential.

$$\begin{aligned} E_{\mathrm{sun}} &= E_{\mathrm{sun,max}} * 2^{-\left(\frac{\psi_{\mathrm{leaf}}}{\psi_{50}}\right)^{c_k}} \\ E_{\mathrm{shade}} &= E_{\mathrm{shade,max}} * 2^{-\left(\frac{\psi_{\mathrm{leaf}}}{\psi_{50}}\right)^{c_k}} \end{aligned} \tag{A15}$$

We define f_w as the ratio of attenuated stomatal conductance ($g_{s,\mathrm{sun}}$, $g_{s,\mathrm{shade}}$) to maximal stomatal conductance ($g_{s,\mathrm{sun,max}}$, $g_{s,\mathrm{shade,max}}$), where $g_{s,\mathrm{sun,max}}$ and $g_{s,\mathrm{shade,max}}$ are the stomatal conductance values associated with $E_{\mathrm{sun,max}}$ and $E_{\mathrm{shade,max}}$. As such, the definition in the main text (equation (14)) represents a linear simplification between f_w, stomatal conductance, and transpiration.

$$\begin{aligned} f_{w,\mathrm{sun}} &= \frac{g_{s,\mathrm{sun}}}{g_{s,\mathrm{sun,max}}} \\ f_{w,\mathrm{shade}} &= \frac{g_{s,\mathrm{shade}}}{g_{s,\mathrm{shade,max}}} \end{aligned} \tag{A16}$$

After each PHS iteration, we compute $g_{s,\mathrm{sun}}$ and $g_{s,\mathrm{shade}}$ via equations (A12) and (A13) (which involves iterating for intercellular CO_2 concentration). We then update $g_{s,\mathrm{sun,max}}$ and $g_{s,\mathrm{shade,max}}$ to achieve consistency

between equations (A14) and (A15). At this point $g_{s,\mathrm{sun,max}}$ and $g_{s,\mathrm{shade,max}}$ no longer refer to the values associated with $f_w = 1$ but rather also incorporate the nonlinearity between g_s and f_w. The PHS iteration continues to convergence of f_w (see Figure A1). The numerics have proven to be stable in practice, but future versions may aim to better integrate PHS within the stomatal conductance scheme to improve the coherence of equations (14) and (A16).

$$\begin{aligned} g_{s,\mathrm{sun,max}} &= \frac{g_{s,\mathrm{sun}}}{f_{w,\mathrm{sun}}} \\ g_{s,\mathrm{shade,max}} &= \frac{g_{s,\mathrm{shade}}}{f_{w,\mathrm{shade}}} \end{aligned} \tag{A17}$$

A3. Details of Water Potential Solution

The continuity of water flow through the system yields four equations:

$$\begin{aligned} E_{\mathrm{sun}} &= q_{\mathrm{sun}} \\ E_{\mathrm{shade}} &= q_{\mathrm{shade}} \\ q_{\mathrm{sun}} + q_{\mathrm{shade}} &= q_{\mathrm{stem}} \\ q_{\mathrm{stem}} &= \sum_{i=1}^{nlevsoi} q_{\mathrm{sr},i} \end{aligned} \tag{A18}$$

We seek the set of vegetation water potential values (four unknowns),

$$\psi = \begin{bmatrix} \psi_{\mathrm{sunleaf}} \\ \psi_{\mathrm{shadeleaf}} \\ \psi_{\mathrm{stem}} \\ \psi_{\mathrm{root}} \end{bmatrix} \tag{A19}$$

that satisfies these equations, as forced by the soil moisture and atmospheric state.

Each flux on the schematic can be represented in terms of the relevant water potentials.

Defining the transpiration fluxes,

$$\begin{aligned} E_{\mathrm{sun}} &= E_{\mathrm{sun,max}} \cdot 2^{-\left(\frac{\psi_{\mathrm{sunleaf}}}{p50}\right)^{c_k}} \\ E_{\mathrm{shade}} &= E_{\mathrm{shade,max}} \cdot 2^{-\left(\frac{\psi_{\mathrm{shadeleaf}}}{p50}\right)^{c_k}} \end{aligned} \tag{A20}$$

Defining the water supply fluxes,

$$\begin{aligned} q_{\mathrm{sun}} &= k_{\mathrm{leaf,max}} \cdot 2^{-\left(\frac{\psi_{\mathrm{stem}}}{p50}\right)^{c_k}} \cdot \mathrm{LAI}_{\mathrm{sun}} \cdot \left(\psi_{\mathrm{stem}} - \psi_{\mathrm{sunleaf}}\right) \\ q_{\mathrm{shade}} &= k_{\mathrm{leaf,max}} \cdot 2^{-\left(\frac{\psi_{\mathrm{stem}}}{p50}\right)^{c_k}} \cdot \mathrm{LAI}_{\mathrm{shade}} \cdot \left(\psi_{\mathrm{stem}} - \psi_{\mathrm{shadeleaf}}\right) \\ q_{\mathrm{stem}} &= \frac{k_{\mathrm{stem,max}}}{z_2} \cdot 2^{-\left(\frac{\psi_{\mathrm{root}}}{p50}\right)^{c_k}} \cdot \mathrm{SAI} \cdot \left(\psi_{\mathrm{root}} - \psi_{\mathrm{stem}} - \Delta\psi_z\right) \\ q_{\mathrm{root}} &= \sum_{i=1}^{nlevsoi} q_{\mathrm{sr},i} = \sum_{i=1}^{nlevsoi} k_{\mathrm{sr},i} \cdot \mathrm{RAI} \cdot \left(\psi_{\mathrm{soil},i} - \psi_{\mathrm{root}} + \Delta\psi_{z,i}\right) \end{aligned} \tag{A21}$$

In the CLM parameter file, $p50$ and c_k are allowed to vary by flux level (transpiration vs. stem flux vs. root flux), but in our experiment (and on the default CLM parameter file), a single value is used for each. PHS solves for the vector ψ that satisfying water flow continuity as forced by atmospheric state and soil moisture. Due to the model nonlinearity, we use a linearized explicit approach, iterating with Newton's method. The initial guess is the solution for ψ (vector) from the previous time step. The general framework, from iteration m to $m + 1$ is as follows:

$$\begin{aligned} q^{m+1} &= q^m + \frac{\delta q}{\delta \psi}\Delta\psi \\ \psi^{m+1} &= \psi^m + \Delta\psi \end{aligned} \tag{A22}$$

So for our first flux balance equation, which requires sunlit leaf transpiration equal the flux of water from the main stem to the sunlit leaf, we have (at iteration $m + 1$) the following:

$$E_{\text{sun}}^{m+1} = q_{\text{sun}}^{m+1} \tag{A23}$$

This can be linearized to

$$E_{\text{sun}}^{m} + \frac{\delta E_{\text{sun}}}{\delta \psi}\Delta\psi = q_{\text{sun}}^{m} + \frac{\delta q_{\text{sun}}}{\delta \psi}\Delta\psi \tag{A24}$$

and rearranged to be

$$\frac{\delta q_{\text{sun}}}{\delta \psi}\Delta\psi - \frac{\delta E_{\text{sun}}}{\delta \psi}\Delta\psi = E_{\text{sun}}^{m} - q_{\text{sun}}^{m} \tag{A25}$$

And for the other three flux balance equations

$$\begin{aligned} \frac{\delta q_{\text{shade}}}{\delta \psi}\Delta\psi - \frac{\delta E_{\text{sha}}}{\delta \psi}\Delta\psi &= E_{\text{sha}}^{m} - q_{1b}^{m} \\ \frac{\delta q_{\text{stem}}}{\delta \psi}\Delta\psi - \frac{\delta q_{\text{sun}}}{\delta \psi}\Delta\psi - \frac{\delta q_{\text{shade}}}{\delta \psi}\Delta\psi &= q_{\text{sun}}^{m} + q_{\text{shade}}^{m} - q_{\text{stem}}^{m} \\ \frac{\delta q_{\text{soil}}}{\delta \psi}\Delta\psi - \frac{\delta q_{\text{stem}}}{\delta \psi}\Delta\psi &= q_{\text{stem}}^{m} - q_{\text{soil}}^{m} \end{aligned} \tag{A26}$$

Putting all four together in matrix form,

$$\begin{bmatrix} \frac{\delta q_{1a}}{\delta \psi} - \frac{\delta E_{\text{sun}}}{\delta \psi} \\ \frac{\delta q_{1b}}{\delta \psi} - \frac{\delta E_{\text{sha}}}{\delta \psi} \\ \frac{\delta q_{2}}{\delta \psi} - \frac{\delta q_{1a}}{\delta \psi} - \frac{\delta q_{1b}}{\delta \psi} \\ \frac{\delta q_{\text{soil}}}{\delta \psi} - \frac{\delta q_{2}}{\delta \psi} \end{bmatrix} \Delta\psi = \begin{bmatrix} E_{\text{sun}}^{m} - q_{1a}^{m} \\ E_{\text{sha}}^{m} - q_{1b}^{m} \\ q_{1a}^{m} + q_{1b}^{m} - q_{2}^{m} \\ q_{2}^{m} - q_{\text{soil}}^{m} \end{bmatrix} \tag{A27}$$

Now to expand the left-hand side, from vector ψ to the four distinct plant water potential nodes, noting that many derivatives are 0 (e.g., $\frac{\delta E_{\text{sun}}}{\delta \psi_{\text{sha}}} = 0$).

Introducing the notation, $A\Delta\psi = b$

$$\Delta\psi = \begin{bmatrix} \Delta\psi_{\text{sunleaf}} \\ \Delta\psi_{\text{shadeleaf}} \\ \Delta\psi_{\text{stem}} \\ \Delta\psi_{\text{root}} \end{bmatrix} \tag{A28}$$

$$A = \begin{bmatrix} \frac{\delta q_{1a}}{\delta \psi_{sun}} - \frac{\delta E_{sun}}{\delta \psi_{sun}} & 0 & \frac{\delta q_{1a}}{\delta \psi_{stem}} & 0 \\ 0 & \frac{\delta q_{1b}}{\delta \psi_{sha}} - \frac{\delta E_{sha}}{\delta \psi_{sha}} & \frac{\delta q_{1b}}{\delta \psi_{stem}} & 0 \\ -\frac{\delta q_{1a}}{\delta \psi_{sun}} & -\frac{\delta q_{1b}}{\delta \psi_{sha}} & \frac{\delta q_{2}}{\delta \psi_{stem}} - \frac{\delta q_{1a}}{\delta \psi_{stem}} - \frac{\delta q_{1b}}{\delta \psi_{stem}} - \frac{\delta q_{2}}{\delta \psi_{stem}} & \frac{\delta q_{2}}{\delta \psi_{root}} \\ 0 & 0 & \frac{\delta q_{soil}}{\delta \psi_{root}} - \frac{\delta q_{2}}{\delta \psi_{root}} & \end{bmatrix} \tag{A29}$$

$$b = \begin{bmatrix} E_{\text{sun}}^{m} - q_{b1}^{m} \\ E_{\text{sha}}^{m} - q_{b2}^{m} \\ q_{b1}^{m} + q_{b2}^{m} - q_{\text{stem}}^{m} \\ q_{\text{stem}}^{m} - q_{\text{soil}}^{m} \end{bmatrix} \tag{A30}$$

We can compute all the entries for A and b based on the soil potential and maximum transpiration forcings and can solve to find the following:

$$\Delta\psi = A^{-1}b \tag{A31}$$

$$\psi_{m+1} = \psi_m + \Delta\psi \tag{A32}$$

We iterate until $b \rightarrow 0$, signifying water flux balance through the system. The result is a final set of water potentials (ψ_{root}, ψ_{stem}, $\psi_{\text{shadeleaf}}$, and ψ_{sunleaf}) satisfying nondivergent water flux through the system.

A4. Parameter Tuning Exercise

We used a factorial design to create 972 ensemble members based on the parameter values below. We ran PHS simulations for each parameter vector under both AMB and TFE conditions. All simulations used the same initial conditions, which were the result of a previous simulation. We evaluated the ensemble members based on the fit to sap flux observations, selecting that which maximized $R^2_{\text{amb}} + R^2_{\text{tfe}} - RMSE_{\text{amb}} - RMSE_{\text{tfe}}$ (Figure S2).

Stem conductivity, k_{max}: 2E−8, 4E−8, 8E−8 s^{-1}
Root conductivity, $k_{r,\text{max}}$: 2E−9, 6E−8, 18E−9 s^{-1}
Root and stem vulnerability p_{50}: −1.75, −2.25, −2.75 MPa
Stomatal p_{50}: above plus either 0 or 0.5 MPa
Vulnerability shape parameter, c_k: 2.95, 3.95, 5.45 (unitless)
Medlyn slope, g_1: 6, 7 $kPa^{0.5}$
Rooting depth parameter, β: 0.95, 0.98, 0.993 (unitless)

Acknowledgments
Observational data collection is a product of CNPQ grant 457914/2013-0/MCTI/CNPq/FNDCT/LBA/ESECAFLOR and U.K. NERC grant NE/J011002 to A. C. L. d. C. We thank all those involved with data collection and the Museu Paraense Emilio Goeldi in Belem PA, Brazil, for hosting the drought experiment at Caxiuanã National Forest and LBA for underpinning support in Brazil. The experiment was founded, and is led, by P. Meir (University of Edinburgh UK and Australian National University, Australia), with R. F. also contributing substantial data collection and empirical analysis used in this publication. Observational data and model output are available online at the GitHub website (github.com/djk2120/phs). The National Center for Atmospheric Research is sponsored by the National Science Foundation. Computing resources (doi:10.5065/D6RX99HX) were provided by the Climate Simulation Laboratory at NCAR's Computational and Information Systems Laboratory, sponsored by the National Science Foundation and other agencies. D. M. L. was supported in part by the RUBISCO Scientific Focus Area (SFA), which is sponsored by the Regional and Global Climate Modeling (RGCM) Program in the Climate and Environmental Sciences Division (CESD) of the Office of Biological and Environmental Research in the U.S. Department of Energy Office of Science. D. K. was supported in part by the Columbia Distinguished Presidential Fellowship, and would like to acknowledge the Columbia Water Center and the NCAR land model working group for feedback during model development and manuscript preparation. Likewise, the authors acknowledge two anonymous reviewers for insightful comments on an earlier version of this paper.

References

Allen, C. D., Macalady, A. K., Chenchouni, H., Bachelet, D., McDowell, N., Vennetier, M., et al. (2010). A global overview of drought and heat-induced tree mortality reveals emerging climate change risks for forests. *Forest Ecology and Management*, *259*(4), 660–684.
Anderegg, W. R. L. (2015). Spatial and temporal variation in plant hydraulic traits and their relevance for climate change impacts on vegetation. *New Phytologist*, *205*(3), 1008–1014.
Anderegg, W. R. L., Kane, J. M., & Anderegg, L. D. L. (2013). Consequences of widespread tree mortality triggered by drought and temperature stress. *Nature Climate Change*, *3*(1), 30–36.
Anderegg, W. R. L., Konings, A. G., Trugman, A. T., Yu, K., Bowling, D. R., Gabbitas, R., et al. (2018). Hydraulic diversity of forests regulates ecosystem resilience during drought. *Nature*, *561*, 538–541.
Anderegg, W. R. L., Schwalm, C., Biondi, F., Camarero, J. J., Koch, G., Litvak, M., et al. (2015). Pervasive drought legacies in forest ecosystems and their implications for carbon cycle models. *Science*, *349*(6247), 528–532.
Anderegg, W. R. L., Wolf, A., Arango-Velez, A., Choat, B., Chmura, D. J., Jansen, S., et al. (2017). Plant water potential improves prediction of empirical stomatal models. *PLOS ONE*, *12*(10), 1–17. https://doi.org/10.1371/journal.pone.0185481
Anderegg, W. R. L., Wolf, A., Arango-Velez, A., Choat, B., Chmura, D. J., Jansen, S., et al. (2018). Woody plants optimise stomatal behaviour relative to hydraulic risk. *Ecology Letters*, *21*(7), 968–977. https://doi.org/10.1111/ele.12962
Avissar, R., Silva Dias, P. L., Silva Dias, M. A. F., & Nobre, C. (2002). The large-scale biosphere-atmosphere experiment in Amazonia (LBA): Insights and future research needs. *Journal of Geophysical Research*, *107*(D20), LBA 54–1–LBA 54–6. https://doi.org/10.1029/2002JD002704
Bartlett, M. K., Klein, T., Jansen, S., Choat, B., & Sack, L. (2016). The correlations and sequence of plant stomatal, hydraulic, and wilting responses to drought. *Proceedings of the National Academy of Sciences*, *113*(46), 13098–13103.
Bonan, G. B. (2008). Forests and climate change: Forcings, feedbacks, and the climate benefits of forests. *Science*, *320*(5882), 1444–1449.
Bonan, G. B., Lawrence, P. J., Oleson, K. W., Levis, S., Jung, M., Reichstein, M., et al. (2011). Improving canopy processes in the Community Land Model version 4 (CLM4) using global flux fields empirically inferred from FLUXNET data. *Journal of Geophysical Research*, *116*, G02014. https://doi.org/10.1029/2010JG001593
Bonan, G. B., Williams, M., Fisher, R. A., & Oleson, K. W. (2014). Modeling stomatal conductance in the earth system: Linking leaf water-use efficiency and water transport along the soil-plant-atmosphere continuum. *Geoscientific Model Development*, *7*(5), 2193–2222.
Bouda, M., & Saiers, J. E. (2017). Dynamic effects of root system architecture improve root water uptake in 1-D process-based soil-root hydrodynamics. *Advances in Water Resources*, *110*, 319–334.
Boyer, J. S. (1967). Leaf water potentials measured with a pressure chamber. *Plant Physiology*, *42*(1), 133–137.
Brooks, R. H., & Corey, A. T. (1964). *Hydraulic properties of porous media*. Fort Collins: Colorado State University Hydrology Papers, Colorado State University.
Burgess, S. S. O., Adams, M. A., Turner, N. C., & Ong, C. K. (1998). The redistribution of soil water by tree root systems. *Oecologia*, *115*(3), 306–311. https://doi.org/10.1007/s004420050521
Cai, G., Vanderborght, J., Langensiepen, M., Schnepf, A., Hüging, H., & Vereecken, H. (2018). Root growth, water uptake, and sap flow of winter wheat in response to different soil water conditions. *Hydrology and Earth System Sciences*, *22*(4), 2449–2470.
Celia, M. A., Bouloutas, E. T., & Zarba, R. L. (1990). A general mass-conservative numerical solution for the unsaturated flow equation. *Water Resources Research*, *26*(7), 1483–1496.
Choat, B., Jansen, S., Brodribb, T. J., Cochard, H., Delzon, S., Bhaskar, R., et al. (2012). Global convergence in the vulnerability of forests to drought. *Nature*, *491*(7426), 752–5.
Christoffersen, B. O., Gloor, M., Fauset, S., Fyllas, N. M., Galbraith, D. R., Baker, T. R., et al. (2016). Linking hydraulic traits to tropical forest function in a size-structured and trait-driven model (TFS v.1-Hydro). *Geoscientific Model Development*, *9*(11), 4227–4255.
Clapp, R. B., & Hornberger, G. M. (1978). Empirical equations for some soil hydraulic properties. *Water Resources Research*, *14*(4), 601–604. https://doi.org/10.1029/WR014i004p00601
Collatz, G. J., Ball, J. T., Grivet, C., & Berry, J. A. (1991). Physiological and environmental regulation of stomatal conductance, photosynthesis and transpiration: A model that includes a laminar boundary layer. *Agricultural and Forest Meteorology*, *54*(2), 107–136.

Cowan, I. R., & Farquhar, G. (1977). Stomatal function in relation to leaf metabolism and environment. *Symposia of the Society for Experimental Biology*, *31*, 471–505.

da Costa, A. C. L., Galbraith, D., Almeida, S., Takeshi, B., Portela, T., da Costa, M., et al. (2010). Effect of 7 yr of experimental drought on vegetation dynamics and biomass storage of an eastern Amazonian rainforest. *The New Phytologist*, *187*(3), 579–591.

da Costa, A. C. L., Metcalfe, D. B., Doughty, C. E., de Oliveira, A. A. R., Neto, G. F. C., da Costa, M. C., et al. (2014). Ecosystem respiration and net primary productivity after 8-10 years of experimental through-fall reduction in an eastern Amazon forest. *Plant Ecology & Diversity*, *7*(1-2), 7–24.

Dai, Y., Dickinson, R. E., & Wang, Y.-P. (2004). A two-big-leaf model for canopy temperature, photosynthesis, and stomatal conductance. *Journal of Climate*, *17*(12), 2281–2299.

De Kauwe, M. G., Kala, J., Lin, Y.-S., Pitman, A. J., Medlyn, B. E., Duursma, R. A., et al. (2015). A test of an optimal stomatal conductance scheme within the CABLE land surface model. *Geoscientific Model Development*, *8*(2), 431–452.

De Kauwe, M. G., Medlyn, B. E., Knauer, J., & Williams, C. A. (2017). Ideas and perspectives: How coupled is the vegetation to the boundary layer? *Biogeosciences*, *14*(19), 4435–4453.

Drake, J. E., Power, S. A., Duursma, R. A., Medlyn, B. E., Aspinwall, M. J., Choat, B., et al. (2017). Stomatal and non-stomatal limitations of photosynthesis for four tree species under drought: A comparison of model formulations. *Agricultural and Forest Meteorology*, *247*, 454–466.

Egea, G., Verhoef, A., & Vidale, P. L. (2011). Towards an improved and more flexible representation of water stress in coupled photosynthesis-stomatal conductance models. *Agricultural and Forest Meteorology*, *151*(10), 1370–1384.

Epila, J., De Baerdemaeker, N. J. F., Vergeynst, L. L., Maes, W. H., Beeckman, H., & Steppe, K. (2017). Capacitive water release and internal leaf water relocation delay drought-induced cavitation in African Maesopsis eminii. *Tree Physiology*, *37*(4), 481–490. https://doi.org/10.1093/treephys/tpw128

Farquhar, G. D., von Caemmerer, S., & Berry, J. A. (1980). A biochemical model of photosynthetic CO_2 assimilation in leaves of C_3 species. *Planta*, *149*(1), 78–90.

Ficklin, D. L., & Novick, K. A. (2017). Historic and projected changes in vapor pressure deficit suggest a continental-scale drying of the United States atmosphere. *Journal of Geophysical Research: Atmospheres*, *122*, 2061–2079. https://doi.org/10.1002/2016JD025855

Fisher, R. A., Williams, M., Costa, A. L. Da, Malhi, Y., Costa, R. F. D., Almeida, S., & Meir, P. (2007). The response of an Eastern Amazonian rain forest to drought stress: Results and modelling analyses from a throughfall exclusion experiment. *Global Change Biology*, *13*(11), 2361–2378. https://doi.org/10.1111/j.1365-2486.2007.01417.x

Fisher, R. A., Williams, M., de Lourdes Ruivo, M., de Costa, A. L., & Meir, P. (2008). Evaluating climatic and soil water controls on evapotranspiration at two Amazonian rainforest sites. *Agricultural and Forest Meteorology*, *148*(6), 850–861.

Fisher, R. A., Williams, M., Do Vale, R. L., Da Costa, A. L., & Meir, P. (2006). Evidence from Amazonian forests is consistent with isohydric control of leaf water potential. *Plant, Cell & Environment*, *29*(2), 151–165. https://doi.org/10.1111/j.1365-3040.2005.01407.x

Flexas, J., Barbour, M. M., Brendel, O., Cabrera, H. M., Carriquí, M., Díaz-Espejo, A., et al. (2012). Mesophyll diffusion conductance to CO_2: An unappreciated central player in photosynthesis. *Plant Science*, *193-194*, 70–84.

Flexas, J., Bota, J., Loreto, F., Cornic, G., & Sharkey, T. D. (2004). Diffusive and metabolic limitations to photosynthesis under drought and salinity in C3 plants. *Plant Biology*, *6*(3), 269–279. https://doi.org/10.1055/s-2004-820867

Franks, P. J., Bonan, G. B., Berry, J. A., Lombardozzi, D. L., Holbrook, N. M., Herold, N., & Oleson, K. W. (2018). Comparing optimal and empirical stomatal conductance models for application in Earth system models. *Global Change Biology*, *24*(12), 5708–5723.

Friedlingstein, P., Meinshausen, M., Arora, V. K., Jones, C. D., Anav, A., Liddicoat, S. K., & Knutti, R. (2014). Uncertainties in CMIP5 climate projections due to carbon cycle feedbacks. *Journal of Climate*, *27*(2), 511–526.

Gentine, P., Entekhabi, D., Chehbouni, A., Boulet, G., & Duchemin, B. (2007). Analysis of evaporative fraction diurnal behaviour. *Agricultural and Forest Meteorology*, *143*(1), 13–29.

Gentine, P., Entekhabi, D., & Polcher, J. (2011). The diurnal behavior of evaporative fraction in the soil-vegetation-atmospheric boundary layer continuum. *Journal of Hydrometeorology*, *12*(6), 1530–1546. https://doi.org/10.1175/2011JHM1261.1

Gentine, P., Guérin, M., Uriarte, M., McDowell, N. G., & Pockman, W. T. (2016). An allometry-based model of the survival strategies of hydraulic failure and carbon starvation. *Ecohydrology*, *9*(3), 529–546. https://doi.org/10.1002/eco.1654

Giardina, F., Konings, A. G., Kennedy, D., Alemohammad, S. H., Oliveira, R. S., Uriarte, M., & Gentine, P. (2018). Tall Amazonian forests are less sensitive to precipitation variability. *Nature Geoscience*, *11*(6), 405–409.

Grant, J. P., Wigneron, J.-P., Jeu, R. A. M. D., Lawrence, H., Mialon, A., Richaume, P., et al. (2016). Comparison of SMOS and AMSR-E vegetation optical depth to four MODIS-based vegetation indices. *Remote Sensing of Environment*, *172*, 87–100.

Green, J. K., Konings, A. G., Alemohammad, S. H., Berry, J., Entekhabi, D., Kolassa, J., et al. (2017). Regionally strong feedbacks between the atmosphere and terrestrial biosphere. *Nature Geoscience*, *10*(6), 410–414.

Harley, P. C., Thomas, R. B., Reynolds, J. F., & Strain, B. R. (1992). Modelling photosynthesis of cotton grown in elevated CO_2. *Plant Cell Environment*, *15*(3), 271–282.

Holbrook, N. M., Ahrens, E. T., Burns, M. J., & Zwieniecki, M. A. (2001). In vivo observation of cavitation and embolism repair using magnetic resonance imaging. *Plant Physiology*, *126*(1), 27–31.

Huntingford, C., Zelazowski, P., Galbraith, D., Mercado, L. M., Sitch, S., Fisher, R., et al. (2013). Simulated resilience of tropical rainforests to CO_2-induced climate change. *Nature Geoscience*, *6*(4), 268–273.

Jackson, R. B., Canadell, J., Ehleringer, J. R., Mooney, H. A., Sala, O. E., & Schulze, E. D. (1996). A global analysis of root distributions for terrestrial biomes. *Oecologia*, *108*(3), 389–411.

Jackson, R. B., Sperry, J. S., & Dawson, T. E. (2000). Root water uptake and transport: Using physiological processes in global predictions. *Trends in Plant Science*, *5*(11), 482–488.

Jarvis, N. J. (2011). Simple physics-based models of compensatory plant water uptake: Concepts and eco-hydrological consequences. *Hydrology and Earth System Sciences*, *15*(11), 3431–3446.

Joetzjer, E., Delire, C., Douville, H., Ciais, P., Decharme, B., Fisher, R., et al. (2014). Predicting the response of the Amazon rainforest to persistent drought conditions under current and future climates: A major challenge for global land surface models. *Geoscientific Model Development*, *7*(6), 2933–2950.

Kattge, J., Díaz, S., Lavorel, S., Prentice, I. C., Leadley, P., Bonisch, G., et al. (2011). TRY—A global database of plant traits. *Global Change Biology*, *17*(9), 2905–2935. https://doi.org/10.1111/j.1365-2486.2011.02451.x

Klein, T., & Niu, S. (2014). The variability of stomatal sensitivity to leaf water potential across tree species indicates a continuum between isohydric and anisohydric behaviours. *Functional Ecology*, *28*(6), 1313–1320. https://doi.org/10.1111/1365-2435.1 2289

Konings, A. G., & Gentine, P. (2017). Global variations in ecosystem-scale isohydricity. *Global Change Biology*, *23*(2), 891–905. https://doi.org/10.1111/gcb.13389

Konings, A. G., Piles, M., Rötzer, K., McColl, K. A., Chan, S. K., & Entekhabi, D. (2016). Vegetation optical depth and scattering albedo retrieval using time series of dual-polarized l-band radiometer observations. *Remote Sensing of Environment*, *172*, 178–189.

Konings, A. G., Williams, A. P., & Gentine, P. (2017). Sensitivity of grassland productivity to aridity controlled by stomatal and xylem regulation. *Nature Geoscience*, *10*(4), 284–288.

Kotowska, M. M., Hertel, D., Rajab, Y. A., Barus, H., & Schuldt, B. (2015). Patterns in hydraulic architecture from roots to branches in six tropical tree species from cacao agroforestry and their relation to wood density and stem growth. *Frontiers in Plant Science*, *6*, 191. https://doi.org/10.3389/fpls.2015.00191

Lee, J.-E., Oliveira, R. S., Dawson, T. E., & Fung, I. (2005). Root functioning modifies seasonal climate. *Proceedings of the National Academy of Sciences of the United States of America*, *102*(49), 17576–17581.

Lemordant, L., Gentine, P., Swann, A. S., Cook, B. I., & Scheff, J. (2018). Critical impact of vegetation physiology on the continental hydrologic cycle in response to increasing CO_2. Proceedings of the National Academy of Sciences.

Lin, C., Gentine, P., Huang, Y., Guan, K., Kimm, H., & Zhou, S. (2018). Diel ecosystem conductance response to vapor pressure deficit is suboptimal and independent of soil moisture. *Agricultural and Forest Meteorology*, *250-251*, 24–34.

Mackay, D. S., Roberts, D. E., Ewers, B. E., Sperry, J. S., McDowell, N. G., & Pockman, W. T. (2015). Interdependence of chronic hydraulic dysfunction and canopy processes can improve integrated models of tree response to drought. *Water Resources Research*, *51*, 6156–6176. https://doi.org/10.1002/2015WR017244

Manzoni, S., Vico, G., Katul, G., Palmroth, S., Jackson, R. B., & Porporato, A. (2013). Hydraulic limits on maximum plant transpiration and the emergence of the safety-efficiency trade-off. *New Phytologist*, *198*(1), 169–178. https://doi.org/10.1111/nph.12126

Manzoni, S., Vico, G., Palmroth, S., Porporato, A., & Katul, G. (2013). Optimization of stomatal conductance for maximum carbon gain under dynamic soil moisture. *Advances in Water Resources*, *62*, 90–105.

McDowell, N. G., & Allen, C. D. (2015). Darcy's law predicts widespread forest mortality under climate warming. *Nature Climate Change*, *5*(7), 669–672.

McDowell, N., Allen, C. D., Anderson-Teixeira, K., Brando, P., Brienen, R., Chambers, J., et al. (2018). Drivers and mechanisms of tree mortality in moist tropical forests. *New Phytologist*, *219*(3), 851–869. https://doi.org/10.1111/nph.15027

McDowell, N. G., Williams, A. P., Xu, C., Pockman, W. T., Dickman, L. T., Sevanto, S., et al. (2016). Multi-scale predictions of massive conifer mortality due to chronic temperature rise. *Nature Climate Change*, *6*, 295–300.

Medlyn, B. E., Duursma, R. A., Eamus, D., Ellsworth, D. S., Prentice, I. C., Barton, C. V. M., et al. (2011). Reconciling the optimal and empirical approaches to modelling stomatal conductance. *Global Change Biology*, *17*(6), 2134–2144. https://doi.org/10.1111/j.1365-2486.2010.02375.x

Meinzer, F. C., Johnson, D. M., Lachenbruch, B., McCulloh, K. A., & Woodruff, D. R. (2009). Xylem hydraulic safety margins in woody plants: Coordination of stomatal control of xylem tension with hydraulic capacitance. *Functional Ecology*, *23*(5), 922–930.

Momen, M., Wood, J. D., Novick, K. A., Pangle, R., Pockman, W. T., McDowell, N. G., & Konings, A. G. (2017). Interacting effects of leaf water potential and biomass on vegetation optical depth. *Journal of Geophysical Research: Biogeosciences*, *122*, 3031–3046. https://doi.org/10.1002/2017JG004145

Nepstad, D. C., de Carvalho, R., Davidson, E. A., Jipp, P. H., Lefebvre, P. A., Negreiros, G. H., et al. (1994). The role of deep roots in the hydrological and carbon cycles of Amazonian forests and pastures. *Nature*, *372*(6507), 666.

Novick, K. A., Ficklin, D. L., Stoy, P. C., Williams, C. A., Bohrer, G., Oishi, A, et al. (2016). The increasing importance of atmospheric demand for ecosystem water and carbon fluxes. *Nature Climate Change*, *6*(11), 1023–1027.

Novick, K. A., Miniat, C. F., & Vose, J. M. (2016). Drought limitations to leaf-level gas exchange: Results from a model linking stomatal optimization and cohesion-tension theory. *Plant, Cell & Environment*, *39*(3), 583–596.

Oleson, K. W., Lawrence, D. M., Bonan, G. B., Drewniak, B., Huang, M., Koven, C. D., et al. (2013). Technical description of version 4.5 of the Community Land Model (CLM), NCAR Tech. Note NCAR/TN-503+STR. National Center for Atmospheric Research, Boulder, Colorado, 420 pp.

Oliveira, R. S., Dawson, T. E., Burgess, S. S. O., & Nepstad, D. C. (2005). Hydraulic redistribution in three amazonian trees. *Oecologia*, *145*(3), 354–363.

Powell, T. L., Galbraith, D. R., Christoffersen, B. O., Harper, A., Imbuzeiro, H. M. A., Rowland, L., et al. (2013). Confronting model predictions of carbon fluxes with measurements of amazon forests subjected to experimental drought. *New Phytologist*, *200*(2), 350–365.

Powell, T. L., Wheeler, J. K., de Oliveira, A. A. R., da Costa, A. C., Saleska, S. R., Meir, P., & Moorcroft, P. R. (2018). Differences in xylem and leaf hydraulic traits explain differences in drought tolerance among mature amazon rainforest trees. *Global Change Biology*, *23*(10), 4280–4293. https://doi.org/10.1111/gcb.13731

Restaino, C. M., Peterson, D. L., & Littell, J. (2016). Increased water deficit decreases Douglas fir growth throughout western US forests. *Proceedings of the National Academy of Sciences*, *113*(34), 9557–9562.

Restrepo-Coupe, N., Levine, N. M., Christoffersen, B. O., Albert, L. P., Wu, J., Costa, M. H., et al. (2017). Do dynamic global vegetation models capture the seasonality of carbon fluxes in the amazon basin? A data-model intercomparison. *Global Change Biology*, *23*(1), 191–208.

Rogers, A., Medlyn, B. E., Dukes, J. S., Bonan, G., Caemmerer, S., Dietze, M. C., et al. (2017). A roadmap for improving the representation of photosynthesis in Earth system models. *New Phytologist*, *213*(1), 22–42. https://doi.org/10.1111/nph.14283

Sack, L., Melcher, P. J., Zwieniecki, M. A., & Holbrook, N. M. (2002). The hydraulic conductance of the angiosperm leaf lamina: A comparison of three measurement methods. *Journal of Experimental Botany*, *53*(378), 2177–2184.

Seager, R., Hooks, A., Williams, A. P., Cook, B., Nakamura, J., & Henderson, N. (2015). Climatology, variability, and trends in the U.S. vapor pressure deficit, an important fire-related meteorological quantity. *Journal of Applied Meteorology and Climatology*, *54*(6), 1121–1141.

Sellers, P. J., Randall, D. A., Collatz, G. J., Berry, J. A., Field, C. B., Dazlich, D. A., et al. (1996). a revised land surface parameterization (SiB2) for atmospheric GCMs. Part I: Model formulation. *Journal of Climate*, *9*(4), 676–705.

Sellers, P. J., Tucker, C. J., Collatz, G. J., Los, S. O., Justice, C. O., Dazlich, D. A., & Randall, D. A. (1996). A revised land surface parameterization (SiB2) for atmospheric GCMs. Part II: The generation of global fields of terrestrial biophysical parameters from satellite data. *Journal of Climate*, *9*(4), 706–737.

Seneviratne, S. I., Lüthi, D., Litschi, M., & Schär, C. (2006). Land-atmosphere coupling and climate change in Europe. *Nature*, *443*(7108), 205–9.

Simonin, K. A., Burns, E., Choat, B., Barbour, M. M., Dawson, T. E., & Franks, P. J. (2015). Increasing leaf hydraulic conductance with transpiration rate minimizes the water potential drawdown from stem to leaf. *Journal of Experimental Botany*, *66*(5), 1303–1315.

Sperry, J. S., Adler, F. R., Campbell, G. S., & Comstock, J. P. (1998). Limitation of plant water use by rhizosphere and xylem conductance: Results from a model. *Plant Cell Environment*, *21*(4), 347–359. https://doi.org/10.1046/j.1365-3040.1998.00287.x

Sperry, J. S., & Love, D. M. (2015). What plant hydraulics can tell us about responses to climate-change droughts. *New Phytologist*, *207*(1), 14–27. https://doi.org/10.1111/nph.13354

Sperry, J. S., Venturas, M. D., Anderegg, W. R. L., Mencuccini, M., Mackay, D. S., Wang, Y., & Love, D. M. (2017). Predicting stomatal responses to the environment from the optimization of photosynthetic gain and hydraulic cost. *Plant, Cell & Environment*, *40*(6), 816–830. https://doi.org/10.1111/pce.12852

Stocker, B. D., Zscheischler, J., Keenan, T. F., Prentice, I. C., Peñuelas, J., & Seneviratne, S. I. (2018). Quantifying soil moisture impacts on light use efficiency across biomes. *New Phytologist*, *218*(4), 1430–1449. https://doi.org/10.1111/nph.15123

Tang, J., Riley, W. J., & Niu, J. (2015). Incorporating root hydraulic redistribution in CLM4.5: Effects on predicted site and global evapotranspiration, soil moisture, and water storage. *Journal of Advances in Modeling Earth Systems*, *7*, 1828–1848. https://doi.org/10.1002/2015MS000484

Tardieu, F., & Simonneau, T. (1998). Variability among species of stomatal control under fluctuating soil water status and evaporative demand: Modelling isohydric and anisohydric behaviours. *Journal of Experimental Botany*, *49*, 419–432.

Thornton, P. E., & Zimmermann, N. E. (2007). An improved canopy integration scheme for a land surface model with prognostic canopy structure. *Journal of Climate*, *20*(15), 3902–3923. https://doi.org/10.1175/JCLI4222.1

Trugman, A. T., Medvigy, D., Mankin, J. S., & Anderegg, W. R. L. (2018). Soil moisture stress as a major driver of carbon cycle uncertainty. *Geophysical Research Letters*, *45*, 6495–6503. https://doi.org/10.1029/2018GL078131

Tyree, M. T., & Sperry, J. S. (1989). Vulnerability of xylem to cavitation and embolism. *Annual Review of Plant Physiology and Plant Molecular Biology*, *40*(1), 19–36.

Ukkola, A. M., Kauwe, M. G. D., Pitman, A. J., Best, M. J., Abramowitz, G., Haverd, V., et al. (2016). Land surface models systematically overestimate the intensity, duration and magnitude of seasonal-scale evaporative droughts. *Environmental Research Letters*, *11*(10), 104012.

Verhoef, A., & Egea, G. (2014). Modeling plant transpiration under limited soil water: Comparison of different plant and soil hydraulic parameterizations and preliminary implications for their use in land surface models. *Agricultural and Forest Meteorology*, *191*, 22–32.

Warren, J. M., Hanson, P. J., Iversen, C. M., Kumar, J., Walker, A. P., & Wullschleger, S. D. (2015). Root structural and functional dynamics in terrestrial biosphere models—Evaluation and recommendations. *New Phytologist*, *205*(1), 59–78. https://doi.org/10.1111/nph.13034

Williams, A. P., Allen, C. D., Macalady, A. K., Griffin, D., Woodhouse, C. A., Meko, D. M., et al. (2013). Temperature as a potent driver of regional forest drought stress and tree mortality. *Nature Climate Change*, *3*(3), 292–297.

Williams, M., Law, B. E., Anthoni, P. M., & Unsworth, M. H. (2001). Use of a simulation model and ecosystem flux data to examine carbon-water interactions in ponderosa pine. *Tree Physiology*, *21*(5), 287–298.

Williams, M., Rastetter, E. B., Fernandes, D. N., Goulden, M. L., Wofsy, S. C., Shaver, G. R., et al. (1996). Modelling the soil-plant-atmosphere continuum in a Quercus-Acer stand at Harvard Forest: The regulation of stomatal conductance by light, nitrogen and soil/plant hydraulic properties. *Plant, Cell & Environment*, *19*(8), 911–927. https://doi.org/10.1111/j.1365-3040.1996.tb00456.x

Wolf, A., Anderegg, W. R. L., & Pacala, S. W. (2016). Optimal stomatal behavior with competition for water and risk of hydraulic impairment. *Proceedings of the National Academy of Sciences*, *113*(46), E7222–E7230.

Xu, X., Medvigy, D., Powers, J. S., Becknell, J. M., & Guan, K. (2016). Diversity in plant hydraulic traits explains seasonal and inter-annual variations of vegetation dynamics in seasonally dry tropical forests. *New Phytologist*, *212*(1), 80–95. https://doi.org/10.1111/nph.14009

Zhou, S., Duursma, R. A., Medlyn, B. E., Kelly, J. W. G., & Prentice, I. C. (2013). How should we model plant responses to drought? An analysis of stomatal and non-stomatal responses to water stress. *Agricultural and Forest Meteorology*, *182-183*, 204–214.